https://doi.org/10.5194/wes-2025-219
Preprint. Discussion started: 6 November 2025

eawe european academy of wind energy
Open Access WIND ENERGY SCIENCE DISCUSSIONS

Damage identification on a large-scale wind turbine rotor blade using sample-based deterministic model updating

Marlene Wolniak[1], Jasper Ragnitz[1], Clemens Jonscher[1], Benedikt Hofmeister[2], Helge Jauken[1], Clemens Hübler[3], and Raimund Rolfes[1]

[1]Leibniz University Hannover / ForWind, Institute of Structural Analysis, Appelstr. 9A, D-30167 Hannover, Germany
[2]Ruhr-University Bochum, Photonics and Terahertz Technology, Universitätsstr. 150, D-44801 Bochum, Germany
[3]Technical University of Darmstadt, Institute of Structural Mechanics and Design, Franziska-Braun-Str. 3, D-64287 Darmstadt, Germany

Correspondence: Marlene Wolniak (m.wolniak@isd.uni-hannover.de)

Abstract. Wind turbine rotor blades are among the most critical components of wind turbines, with their structural integrity directly affecting reliability, lifetime, and maintenance costs. Reliable damage identification is therefore essential for structural health monitoring (SHM) strategies in wind energy applications. In this context, the updating of numerical models represents an established method for vibration-based non-destructive damage identification, including damage detection, localization and quantification. Naturally, the model-updating process is affected by different sources of uncertainty. On the one hand, the numerical model always represents an idealization that introduces unavoidable discrepancies between its basic assumptions and reality. On the other hand, the measurement data and identified modal parameters, typically serving as damage-sensitive features, are subject to uncertainty. Despite extensive research on uncertainty quantification and propagation in model updating, comparative studies of model-updating procedures applied to large-scale structures, particularly wind turbine rotor blades, remain scarce. Moreover, the level of model fidelity and the impact of different design variable configurations associated with the selected numerical model are seldom examined in the context of model updating, typically formulated as an optimization procedure.

This study addresses this gap by systematically evaluating how model fidelity and design variable parameterization influence the model-updating results while considering uncertainty associated with the measurement data and identification process. The investigations are conducted using measurement data from a $31\,\mathrm{m}$ rotor blade subjected to edgewise fatigue loading. A comparison of the results shows that all design variable configurations yield consistent results, confirming the robustness of the presented model-updating procedures. Model fidelity, however, strongly influences the outcomes, with higher accuracy and detail leading to distinctly improved damage identification.

1 Introduction

The structural integrity of wind turbine rotor blades directly affects the operational reliability, energy yield, service lifetime, and maintenance costs of entire wind farms (Hau, 2013). The blades are typically highly loaded and critical to the overall design of the turbine (Kong et al., 2023). With the continuous upscaling of turbine and blade size, rotor blades are increasingly

https://doi.org/10.5194/wes-2025-219
Preprint. Discussion started: 6 November 2025

eawe european academy of wind energy
Open Access WIND ENERGY SCIENCE DISCUSSIONS

exposed to fatigue loads, making them susceptible to damage initiation and crack propagation. Algolfat et al. (2023) give an overview of common damage scenarios for wind turbine rotor blades and point out that such types of damage can lead to failure or breakdown of the wind turbines as they increase the level of vibrations and impose additional dynamic loads. Consequently, reliable identification and characterization of blade damage is essential for effective structural health monitoring (SHM) strategies in wind energy applications (Yang et al., 2017; Kaewniam et al., 2022).

Within an SHM framework, the basic assumption is that damage, defined as degradation of the mechanical properties (Worden et al., 2007), causes detectable changes in the structural dynamic behavior (Mottershead and Friswell, 1993). Hence, to enable damage identification, including detection, localization and quantification, vibration measurement data need to be acquired for at least two different states of the considered structure (Friswell, 2007), meaning a reference state and an analysis (i.e., target) state. A variety of different SHM methods based on various damage-sensitive features have been developed and applied to date (Avci et al., 2021). Such approaches are of vital importance when seeking to maintain the safety and integrity of the structures under consideration (Brownjohn, 2007; Fan and Qiao, 2011). Among them, the updating of numerical models represents an established vibration-based non-destructive damage identification technique (Das et al., 2016; Ereiz et al., 2022), which is also employed within this work. Due to its methodology, the model-updating process is affected by two major sources of uncertainty – associated with the model and the measurement data – as clearly pointed out by Simoen et al. (2015).

One source of uncertainty arises from the numerical model employed in the updating procedure. Depending on its level of fidelity, in terms of the chosen finite element (FE) type, the numerical model represents a more or less simplified version of the structure under consideration and, by definition, always remains an idealization. Consequently, a certain level of discrepancy between the model predictions and the corresponding characteristics identified from the measurement data is inevitable (Mottershead et al., 2011). With regard to the modeling of (wind turbine) rotor blades, extensive research has been conducted on the comparison of numerical models based on different FE types and, thus, with varying levels of model fidelity (Lake and Nixon, 1988; Volovoi et al., 2001; Peeters et al., 2018; de Almeida et al., 2025). However, comparative analyses of model-updating procedures applied to large-scale structures, especially to wind turbine rotor blades, using different numerical models and associated design variable configurations remain scarce. Mostly, model-updating procedures applied to small- or large-scale wind turbine rotor blades utilize FE beam models (Noever-Castelos et al., 2022; Turnbull and Omenzetter, 2024). Chetan et al. (2021), for example, propose a multi-fidelity digital twin model for the simulation of a $21\,\mathrm{m}$ sub-scale wind turbine rotor blade but perform the actual updating of the mass and stiffness distributions using an Euler-Bernoulli beam model. Moreover, the application of detailed shell-based models for model updating allowing for damage identification along the blade span and chord is rarely published. Knebusch et al. (2020) applied a gradient-based model-updating procedure to a $20\,\mathrm{m}$ rotor blade using a detailed shell model. However, the design variables were mapped directly to material properties of so-called predefined design fields, representing FE groups. While this is a common approach to keep the number of design variables low (Levin and Lieven, 1998), it is dependent on a prior grouping of FEs and can result in undesired oscillatory stiffness distributions when an unconstrained formulation is used.

Another source of uncertainty is the measurement data. Due to the unavoidable spatial sparsity and noisiness of sensor signals and possible imperfections in the measurement equipment, measured data always contain uncertainty, which can merely

https://doi.org/10.5194/wes-2025-219
Preprint. Discussion started: 6 November 2025

eawe european academy of wind energy
Open Access WIND ENERGY SCIENCE DISCUSSIONS

be minimized but never fully eliminated (Link, 1999). In addition to the uncertainty contained in the raw measurement data, further uncertainty is introduced during the subsequent signal processing and identification of modal characteristics of the physical structure (Friswell and Mottershead, 1995), which is referred to as identification uncertainty. In recent years, numerous studies have investigated uncertainty quantification and propagation in model updating, employing methods such as Bayesian inference (Bi et al., 2021), interval approaches and fuzzy logic (Faes and Moens, 2020), and the sample-based deterministic model-updating (SDMU) approach recently introduced by the authors (Wolniak et al., 2025a). However, the primary focus of these works has typically been on methodological development rather than on large-scale experimental validation.

Within this work, the described uncertainty sources inherent to the model-updating process are systematically examined and addressed using a $31\,\mathrm{m}$ laboratory wind turbine rotor blade subjected to edgewise fatigue loading. The rotor blade was instrumented with accelerometers to monitor its gradual stiffness degradation due to the fatigue loading, ultimately leading to crack growth across the leading edge at approximately $8\,\mathrm{m}$ distance from the blade root. The measured acceleration time series along with the corresponding modal properties identified from the measurement data using Bayesian operational modal analysis (BayOMA) (Au et al., 2013) are published in an open-access repository (Wolniak et al., 2025b) alongside this paper. This unique experimental dataset provides a basis for monitoring the gradual stiffness degradation of a large-scale laboratory rotor blade tested under edgewise fatigue loading.

An outstanding feature of this rotor blade fatigue test was the complete documentation of the manufacturing process, accompanied by detailed material and geometry data. This extensive information enabled the development of two numerical models, i.e., a beam model and a shell model, with differing levels of fidelity, both of which are employed and compared within the model-updating procedure(s). Consequently, different design variable configurations are introduced and applied, as their selection depends not only on the purpose of model updating but also on the specific numerical model used in the updating process, including its element type and geometry. In this work, all presented design variable configurations define a one- or two-dimensional damage distribution function used to alter the stiffness properties of the respective numerical model. This definition ensures a smooth, realistic stiffness distribution and is independent of the FE mesh resolution and of prior assumptions about the defect location while requiring few design variables. As in all related studies (Fan and Qiao, 2011; Simoen et al., 2015; Ereiz et al., 2022), this work also uses the discrepancies between simulated and identified modal properties as updating objectives. In particular, the eigenfrequencies and eigenmodes of the large-scale rotor blade are utilized in this work. To avoid the need for weighting factors, multi-objective optimization is applied. In addition, both objective functions are formulated in relative terms, taking into account a possible constant discrepancy between the simulated and identified responses for both the analysis and reference states. To account for the uncertainty associated with the modal properties identified from the measurement data, the SDMU approach is utilized (Wolniak et al., 2025a). This approach is motivated by a separation of the uncertainty incorporation and the model-updating procedure itself, resulting in an approach that is fully adaptable to the specific problem at hand. In this work, an SDMU realization is applied which delivers fully deterministic and reproducible results.

The following key points summarize the fundamental aspects of this study.

- Publication of a unique experimental dataset along with identified modal properties, providing a basis for monitoring the stiffness degradation of a large-scale rotor blade tested under edgewise fatigue loading.

https://doi.org/10.5194/wes-2025-219
Preprint. Discussion started: 6 November 2025

eawe european academy of wind energy
Open Access WIND ENERGY SCIENCE DISCUSSIONS

- Application of a beam and shell model within the model-updating process to compare different levels of fidelity.
- Application of different design variable configurations tailored to the respective numerical models utilized.

The combination of a unique large-scale rotor blade fatigue test, the systematic model updating across the gradual stiffness degradation of the rotor blade and the comparative evaluation of numerical models and associated design variable configurations of different levels of fidelity constitutes a novel contribution in the context of SHM for wind turbine rotor blades. The results demonstrate the methodological robustness of the proposed model-updating procedure, including the SDMU approach that considers uncertainty associated with the measurement data and the subsequent modal parameter identification and including the use of the one- and two-dimensional damage distribution functions parameterized by the different design variable configurations. Moreover, the findings of this work underline the importance of defining the analysis objective in advance, as the choice of the numerical model and the associated design variable parameterization is decisive in obtaining meaningful and reliable results.

2 Model updating

Typically, a model-updating problem is formulated inversely and treated as an optimization problem (Mottershead et al., 2011). An objective function is used to compare the structural dynamic behavior of the numerical model to a target state and an optimization algorithm is used to find a model to match this target state by updating the selected design variables. Most often, this is achieved through stiffness or mass modifications (Friswell and Mottershead, 1995).

The utilized optimization algorithm is essentially designed to solve bounded and nonlinear optimization problems. This can be stated as

$$\text{minimize } \boldsymbol{\varepsilon}(\boldsymbol{x}) \qquad \text{for } \boldsymbol{\varepsilon} \in \mathbb{R}^m, \boldsymbol{x} \in \mathbb{R}^n, \tag{1}$$

where $\boldsymbol{\varepsilon}$ is a vector-valued function consisting of m objective functions $\boldsymbol{\varepsilon}(\boldsymbol{x}) = (\varepsilon_1(\boldsymbol{x}), \varepsilon_2(\boldsymbol{x}), ..., \varepsilon_m(\boldsymbol{x}))$ and $\boldsymbol{x}$ is the n-dimensional vector of design variables. In this work, multi-objective optimization is applied, where the concept of Pareto dominance is followed (Marler and Arora, 2004). The space of the design variables is bounded by the volume of a hypercube

$$\boldsymbol{x}_{\text{lb}} \leq \boldsymbol{x} \leq \boldsymbol{x}_{\text{ub}}, \tag{2}$$

where $\boldsymbol{x}_{\text{lb}}$ and $\boldsymbol{x}_{\text{ub}}$ are the lower and upper bounding vectors, respectively. For the optimization performed in this work, the optimization framework EngiO, introduced by Berger et al. (2021), is utilized.

From Equation 1, it is clear that the optimization process and, thus, the quality of model-updating results depend on two key aspects: On the configuration of the design variables $\boldsymbol{x}$ on the one hand, and, on the other hand, on the formulation of the objective function $\boldsymbol{\varepsilon}(\boldsymbol{x})$. In the following subsections, detailed information is given about the definitions used in this work.

https://doi.org/10.5194/wes-2025-219
Preprint. Discussion started: 6 November 2025

eawe european academy of wind energy
Open Access WIND ENERGY SCIENCE DISCUSSIONS

2.1 Design variables

The determination of the design variables strongly depends on the purpose of model updating. Since the aim of this contribution is damage identification, specifically, damage localization and quantification, the parameterization should be able to identify the geometric position of the damage and its intensity.

As damage mainly manifests itself as a change in stiffness, the general approach for most FE model-updating procedures with the aim of damage identification is to alter the stiffness properties of the model at hand (Friswell and Mottershead, 1995). This approach is also applied in this work. As no prior knowledge of the defect location is assumed, the updating of the stiffness properties of all N_{el} elements is performed, independent of the element type. This is implemented by adapting the initial Young's modulus E_0 of each FE with a corresponding scaling factor θ_k

$$E_{\theta,k} = E_0 \theta_k \qquad \text{with} \quad k \in [1, N_{\mathrm{el}}]. \tag{3}$$

The stiffness scaling factors θ_k are calculated on the basis of the design variables. In this work, the design variables parameterize a so-called damage distribution function, previously introduced and applied by the authors (Wolniak et al., 2023). By formulating the mapping of the considered structural properties to the FEs using a distribution function, a smooth, realistic distribution is ensured. This forces the model-updating process to focus on global structural dynamics instead of over-fitting local deviations. Moreover, the model-updating procedure is independent of the FE mesh resolution and of prior assumptions about the defect location while only needing few design variables. However, applying the damage distribution in its current form restricts damage identification to only one damage position. In this work, a spatial Gaussian damage distribution function is considered based on the assumption that the damage roughly follows this type of distribution.

The determination of the design variables additionally depends on the specific model used in the updating procedure, as its element type and geometry inherently influence their configuration. In this work, two different numerical models of the large-scale rotor blade are considered, which necessitate at least two different design variable configurations. In the following subsections, firstly, the parameterization of a one-dimensional damage distribution function for the model updating using a rather simple beam model of the rotor blade is presented. This definition based on three design variables was already introduced and successfully employed in several preceding publications (Bruns et al., 2019a, b; Wolniak et al., 2023), where deterministic model updating was performed on simulated and experimental application examples. In addition, in this work, the one-dimensional parameterization is extended by a fourth design variable, which independently adjusts the stiffness properties in the edgewise and flapwise directions of the rotor blade, allowing for a distinct consideration of both directions. Secondly, the parameterization of a two-dimensional damage distribution function for the model updating using a more detailed shell model of the rotor blade is introduced. This configuration is based on five design variables and allows for a damage identification in longitudinal direction and circumferential direction.

https://doi.org/10.5194/wes-2025-219
Preprint. Discussion started: 6 November 2025

eawe european academy of wind energy
Open Access WIND ENERGY SCIENCE DISCUSSIONS

2.1.1 One-dimensional damage distribution function – 3 design variables

The one-dimensional damage distribution function is defined along a single control variable, specifically the length L of the beam model representing the rotor blade. It can be described by the three design variables

$$\boldsymbol{x}_{\mathrm{1D}} = (\mu_L \;\; \sigma_L \;\; D_{\mathrm{1D}})^{\mathrm{T}}. \tag{4}$$

In the design variable vector $\boldsymbol{x}_{\mathrm{1D}}$, μ_L represents the geometric position of the distribution function's center point along the length, σ_L represents the width (standard deviation) of the distribution, i.e., the extent of the damage, and D_{1D} represents the intensity of the damage. In this case, the damage intensity is defined as the area under the Gaussian distribution function defined by μ_L and σ_L.

The calculation of the stiffness scaling factors $\theta_{\mathrm{1D},k}$ for each FE with a corresponding length l_k is based on the probability density function $f\left(s_{L,k} \mid \mu_L, \sigma_L\right)$ evaluated along the control variable $s_{L,k}$ and truncated to the interval $0 \leq s_{L,k} \leq L$

$$\theta_{\mathrm{1D},k} = 1 - D_{\mathrm{1D}}\, L\, \frac{f\left(s_{L,k} \mid \mu_L, \sigma_L\right)}{l_k} \qquad \text{with} \quad k \in [1, N_{\mathrm{el}}]. \tag{5}$$

More detailed information regarding the one-dimensional damage distribution function parameterized by three design variables is given in Wolniak et al. (2023).

2.1.2 One-dimensional damage distribution function – 4 design variables

By introducing a fourth design variable $\lambda \in [0, 1]$, the above-described one-dimensional damage distribution function is extended so that it can alter the stiffness properties in flapwise and edgewise directions separately. Therefore, instead of changing the initial Young's modulus E_0 of each FE, which alters each element stiffness altogether, the initial moments of inertia $I_{xx,0}$ and $I_{yy,0}$ in flapwise and edgewise directions and the initial moment of deviation $I_{xy,0}$ are updated separately from each other in an equivalent way to Equation 3

$$\begin{pmatrix} I_{xx,\theta,k} \\ I_{yy,\theta,k} \\ I_{xy,\theta,k} \end{pmatrix} = \begin{pmatrix} I_{xx,0,k} \\ I_{yy,0,k} \\ I_{xy,0,k} \end{pmatrix} \circ \begin{pmatrix} \theta_{xx,\mathrm{1D},k} \\ \theta_{yy,\mathrm{1D},k} \\ \theta_{xy,\mathrm{1D},k} \end{pmatrix} \qquad \text{with} \quad k \in [1, N_{\mathrm{el}}]. \tag{6}$$

The calculation of the stiffness scaling factors $\boldsymbol{\theta}_{\mathrm{1D},k}$ for each of the three moments of inertia follows a similar approach to Equation 5, except that the damage intensity D_{1D} is scaled by different factors λ_{xx}, λ_{yy} and λ_{xy}

$$\begin{pmatrix} \theta_{xx,\mathrm{1D},k} \\ \theta_{yy,\mathrm{1D},k} \\ \theta_{xy,\mathrm{1D},k} \end{pmatrix} = 1 - D_{\mathrm{1D}} \begin{pmatrix} \lambda_{xx} \\ \lambda_{yy} \\ \lambda_{xy} \end{pmatrix} L\, \frac{f\left(s_{L,k} \mid \mu_L, \sigma_L\right)}{l_k} \qquad \text{with} \quad k \in [1, N_{\mathrm{el}}], \tag{7}$$

https://doi.org/10.5194/wes-2025-219
Preprint. Discussion started: 6 November 2025

eawe european academy of wind energy
Open Access WIND ENERGY SCIENCE DISCUSSIONS

whereby these different factors are defined based on the fourth design variable λ

$$\begin{pmatrix} \lambda_{xx} \\ \lambda_{yy} \\ \lambda_{xy} \end{pmatrix} = \begin{pmatrix} \lambda \\ 1-\lambda \\ \sqrt{\lambda(1-\lambda)} \end{pmatrix} \quad \text{with} \quad \lambda \in [0,1]. \tag{8}$$

The presented formulation allows the single design variable λ to capture the trade-off between edgewise and flapwise stiffness. In addition, the total stiffness alteration applied in the different lateral directions of the structure remains proportional to the damage intensity D_{1D}, which is determined and adjusted by the employed optimization algorithm. Consequently, the progression of the model-updating procedure mirrors that of utilizing only three design variables (cf. Section 2.1.1), with the added ability to introduce damage separately in the two lateral directions.

For the calculation of the scaling factor λ_{xy}, it is assumed that the structural stiffness undergoes an affine transformation characterized by independent scaling along the two lateral axes (Timoshenko and Gere, 2012). This preserves the overall shape of the stiffness distribution while modifying its extents along the x (i.e., flapwise) and y (i.e., edgewise) axes. As a result, the scaling factor for the moment of deviation (also referred to as the product of inertia), I_{xy}, can be derived as the geometric mean of the scaling factors for I_{xx} and I_{yy}, i.e., $\lambda_{xy} = \sqrt{\lambda_{xx}\lambda_{yy}} = \sqrt{\lambda(1-\lambda)}$.

2.1.3 Two-dimensional damage distribution function – 5 design variables

Using the shell model as representation of the rotor blade, a parameterization of the damage distribution function along a single control variable, i.e., the length L of the rotor blade, is no longer sufficient. The parameterization has to be extended to a second control variable, meaning the perimeter P of the rotor blade. As a result, a two-dimensional damage distribution function is defined on the surface of the shell model and the design variable vector describing this two-dimensional damage distribution function is extended to five entries

$$\boldsymbol{x}_{2D} = (\mu_L \;\; \sigma_L \;\; \mu_P \;\; \sigma_P \;\; D_{2D})^{\mathrm{T}}. \tag{9}$$

As the damage distribution function is now bell-shaped, its center point is described by the two geometric positions μ_L and μ_P along the length and the perimeter of the rotor blade, respectively

$$\boldsymbol{\mu}_{2D} = \begin{pmatrix} \mu_L \\ \mu_P \end{pmatrix}. \tag{10}$$

As the blade's perimeter changes along its length, the design variable μ_P is normalized to values between $-0.5 < \mu_P \leq 0.5$, whereby the value 0 corresponds to the leading edge (LE) and the values -0.5 and 0.5 correspond to the trailing edge (TE) of

https://doi.org/10.5194/wes-2025-219
Preprint. Discussion started: 6 November 2025

eawe european academy of wind energy
Open Access WIND ENERGY SCIENCE DISCUSSIONS

the rotor blade. The damage extent is characterized by σ_L and σ_P, making up the covariance matrix

$$\boldsymbol{\Sigma}_{\mathrm{2D}} = \begin{pmatrix} \sigma_L & 0 \\ 0 & \sigma_P \end{pmatrix}. \tag{11}$$

The off-diagonal terms are set to zero for the application considered. This leads to a distribution function that can be circular or elliptical but is restricted to have no inclination or obliqueness. The design variable σ_P is normalized in the same manner as μ_P. The damage intensity D_{2D} is defined similarly to the one-dimensional formulation as the area under the (bell-shaped) two-dimensional Gaussian distribution function.

For the two-dimensional application, the calculation of the stiffness scaling factors $\theta_{\mathrm{2D},k}$ for each FE with a corresponding area a_k is based on the probability density function $f(\boldsymbol{s}_k \mid \boldsymbol{\mu}_{\mathrm{2D}}, \boldsymbol{\Sigma}_{\mathrm{2D}})$ evaluated along the two-dimensional control variable $\boldsymbol{s}_k = (s_{L,k} \;\; s_{P,k})^{\mathrm{T}}$

$$\theta_{\mathrm{2D},k} = 1 - D_{\mathrm{2D}}\, A\, \frac{f(\boldsymbol{s}_k \mid \boldsymbol{\mu}_{\mathrm{2D}}, \boldsymbol{\Sigma}_{\mathrm{2D}})}{a_k} \qquad \text{with} \quad k \in [1, N_{\mathrm{el}}]. \tag{12}$$

The two-dimensional control variable $\boldsymbol{s}_k$ is truncated to $0 \leq s_{L,k} \leq L$ along the blade's length and to $-0.5 < s_{P,k} \leq 0.5$ along the normalized perimeter of the blade. A denotes the total area (surface) of the rotor blade.

2.2 Objective function formulation – sample-based deterministic model updating

As uncertainty is inevitable in real-world model-updating applications, the formulation of the model-updating problem is uncertain as well. To tackle the issue of uncertainty propagation within the model-updating procedure, the authors recently introduced the sample-based deterministic model-updating (SDMU) approach (Wolniak et al., 2025a). The key idea behind the SDMU approach is to exclude the uncertainty from the design-variable dependent part of the objective function formulation, i.e., from the actual model-updating procedure. Instead, the uncertainty is incorporated indirectly by generating multiple discrete input samples. Following the sample provision, a fully deterministic model-updating procedure using a numerical optimization algorithm is executed based on each input sample. Thus, multiple deterministic model-updating procedures are performed based on the input samples.

Due to the separation of the uncertainty incorporation and model-updating procedure, both the type of sample provision and the choice of the optimization algorithm are arbitrary. This interchangeability allows the approach to be fully adaptable to the specific problem at hand. Consequently, the SDMU approach can be realized to deliver fully reproducible results, which is also applied within this work. Therefore, the global deterministic optimization algorithm global pattern search (GPS) (Hofmeister et al., 2019) is chosen. As the two modal parameters eigenfrequencies f and eigenmodes φ are considered as the two objectives for the model-updating procedure of the large-scale rotor blade, multi-objective optimization is required. Hence, the multi-objective extension of the deterministic optimization algorithm is utilized, namely the multi-objective global pattern search (MOGPS) (Günther et al., 2025).

https://doi.org/10.5194/wes-2025-219
Preprint. Discussion started: 6 November 2025

eawe european academy of wind energy
Open Access WIND ENERGY SCIENCE DISCUSSIONS

Regarding the sample provision, the available measurement data were segmented into a number of datasets. For each dataset, the eigenfrequency and eigenmode mean values were identified using BayOMA and cross-combined for each considered reference state and analysis state. Thus, after applying this specific (or any other) sample provision (SP), a resulting number of N_{SP} modal parameter samples $f_{\mathrm{M},i,j}$ and $\boldsymbol{\varphi}_{\mathrm{M},i,j}$ with $i \in [1, N_{\mathrm{modes}}]$ and $j \in [1, N_{\mathrm{SP}}]$ represent the input samples for each subsequent deterministic model-updating procedure. The subscript $(\cdot)_{\mathrm{M}}$ denotes measured data, i denotes the mode index, whereby N_{modes} is the number of modes investigated, and j is the sample number. As a result, the two objective functions are each vectors with N_{SP} entries, the first comprising the mean squared eigenfrequency error $\varepsilon_{f,j}$ and the second comprising the mean squared eigenmode error $\varepsilon_{\boldsymbol{\varphi},j}$

$$\boldsymbol{\varepsilon}_j(\boldsymbol{x}) = \begin{cases} \varepsilon_{f,j}(\boldsymbol{x}) = \sqrt{\dfrac{1}{N_{\mathrm{modes}}} \sum_{i=1}^{N_{\mathrm{modes}}} \left(\dfrac{f_{\mathrm{SA},i}(\boldsymbol{x}) - f_{\mathrm{SR},i}}{f_{\mathrm{SR},i}} - \dfrac{f_{\mathrm{MA},i,j} - f_{\mathrm{MR},i,j}}{f_{\mathrm{MR},i,j}} \right)^2} \\ \varepsilon_{\varphi,j}(\boldsymbol{x}) = \sqrt{\dfrac{1}{N_{\mathrm{modes}}} \sum_{i=1}^{N_{\mathrm{modes}}} \left(\dfrac{1}{N_{\mathrm{sensors}}} \sum_{u=1}^{N_{\mathrm{sensors}}} \left((\boldsymbol{\varphi}_{\mathrm{SA},u,i}(\boldsymbol{x}) - \boldsymbol{\varphi}_{\mathrm{SR},u,i}) - (\boldsymbol{\varphi}_{\mathrm{MA},u,i,j} - \boldsymbol{\varphi}_{\mathrm{MR},u,i,j}) \right)^2 \right)^2} \end{cases}$$

$$\text{with} \quad u \in [1, N_{\mathrm{sensors}}], \quad i \in [1, N_{\mathrm{modes}}], \quad j \in [1, N_{\mathrm{SP}}]. \tag{13}$$

The subscript $(\cdot)_{\mathrm{M}}$ indicates a measured quantity, whereas simulated modal parameters are denoted by the subscript $(\cdot)_{\mathrm{S}}$. The subscripts $(\cdot)_{\mathrm{R}}$ and $(\cdot)_{\mathrm{A}}$ indicate the reference state and analysis state, respectively. The presented definition of the two objective functions was introduced by Ragnitz et al. (2025) for damage localization on the LUMO benchmark structure (Wernitz et al., 2022) using a stochastic multi-objective model-updating approach. Both objective functions are based on a relative formulation, which takes into account a possible constant discrepancy between the simulated and identified responses for both the analysis and reference states of the examined structure. The goal is to obtain a numerically efficient, well-formulated optimization problem, which can handle irreducible modeling errors.

One way the N_{SP} two-objective functions $\boldsymbol{\varepsilon}(\boldsymbol{x})$ can be handled is by performing independent model-updating procedures on each of the two-objective functions. However, for high sample numbers and more complex numerical models, this approach will eventually become very expensive in terms of computing time. This is why the use of a meta-model is proposed, whereby the process of setting up and integrating a considered meta-model is incorporated into the SDMU approach and is referred to as metaSDMU (Wolniak et al., 2025a). The objective is to derive a meta-model using a single representative deterministic model-updating procedure in order to generate a sampling pattern within the design variable space, which is dense in the area where the solution(s) are expected. The design variable samples generated during this optimization procedure and the corresponding objective function values calculated provide the training data for the two meta-models – one meta-model for each input, i.e., each modal parameter. Subsequently, these meta-models replace the actual numerical model such that

$$f_{\mathrm{meta,S},i}(\boldsymbol{x}) \approx f_{\mathrm{S},i}(\boldsymbol{x}) \quad \text{and} \quad \boldsymbol{\varphi}_{\mathrm{meta,S},i}(\boldsymbol{x}) \approx \boldsymbol{\varphi}_{\mathrm{S},i}(\boldsymbol{x}) \qquad \text{with} \quad i \in [1, N_{\mathrm{modes}}] \tag{14}$$

holds true for each (simulated) eigenfrequency $f_{\mathrm{S},i}$ and eigenmode $\boldsymbol{\varphi}_{\mathrm{S},i}$.

https://doi.org/10.5194/wes-2025-219
Preprint. Discussion started: 6 November 2025

eawe european academy of wind energy
Open Access WIND ENERGY SCIENCE DISCUSSIONS

This way, the potentially computationally expensive model evaluations required in every iteration step only have to be performed during one model-updating procedure. For all other samples, the model updating with consideration of uncertainty (cf. Equation 13) is performed using the meta-models, which are computationally much more efficient. More detailed information regarding the (meta)SDMU approach is given in Wolniak et al. (2025a).

3 Rotor blade fatigue test

The large-scale destructive rotor blade fatigue test was carried out on a $31\,\mathrm{m}$ wind turbine rotor blade. The blade was manufactured by the Fraunhofer Institute for Wind Energy Systems (Fraunhofer IWES) and the fatigue test took place in one of their test facilities in Bremerhaven, Germany. The fatigue test was carried out by Fraunhofer IWES, while the measurement system setup, data acquisition and subsequent operational modal analysis were conducted by the authors of this work.

During the test, the blade was bolted to an adapter plate with the suction side facing downwards. Figure 1 shows the suspended laboratory rotor blade from different perspectives. Four load shears were mounted on the blade to apply the load and introduce a controllable bending moment. The longitudinal positions and masses of the four load shears are listed in Table 1.

(a) Pressure side. (b) Suction side.

Figure 1. Suspended rotor blade in the test facility in Bremerhaven.

Table 1. Load shear positions and masses.

Load shear	Longitudinal position in m	Mass in kg
1	9	3674
2	15	608
3	20	176
4	29	92

A total of 34 IEPE (integrated electronics piezo-electric) accelerometers with a dynamic range of $\pm 100\,\frac{\mathrm{m}}{\mathrm{s}^2}$ were mounted on the pressure side (facing upwards) of the rotor blade. These accelerometers contain an internal charge amplifier, providing a voltage output proportional to acceleration, which enables high-sensitivity vibration measurements with low signal degradation over long cables. The sensors were placed every $3\,\mathrm{m}$ along the center line and the TE of the blade, as shown in Figure 1a. Two

https://doi.org/10.5194/wes-2025-219
Preprint. Discussion started: 6 November 2025

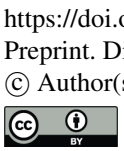

eawe european academy of wind energy
Open Access WIND ENERGY SCIENCE DISCUSSIONS

accelerometers each were fixed at each sensor position at a 90-degree angle to each other in order to measure the flapwise and edgewise directions separately. Figure 2 shows an example sensor setup and in Table 2, the longitudinal sensor positions are listed. As the cross-section of the rotor blade gradually tapers along the blade length, 10 sensor positions were located along the center line and 7 sensor positions were located along the TE.

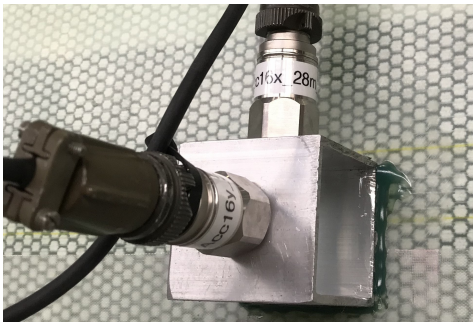

Figure 2. Example sensor setup with two accelerometers at a 90-degree angle.

Table 2. Sensor positions.

Longitudinal position from blade root in m	4	7	10	13	16	19	22	25	28	31
Center line	x	x	x	x	x	x	x	x	x	x
Trailing edge	x	x	x	x	x	x	x			

The fatigue load was introduced by a hydraulic cylinder connected to the second load shear at blade length $L = 15\,\mathrm{m}$. The periodic excitation was carried out in edgewise direction close to the rotor blade's first eigenfrequency in this direction using a frequency of $1.59\,\mathrm{Hz}$. The following fatigue load levels (FLL) were set during the course of the rotor blade fatigue test.

- FLL 1: ≈ 240000 cycles with $\pm 1700\,\mu\varepsilon$ (measured at $L = 12\,\mathrm{m}$)
- FLL 2: ≈ 425000 cycles with $\pm 1900\,\mu\varepsilon$ (measured at $L = 12\,\mathrm{m}$)
- FLL 3: ≈ 11000 cycles with $\pm 2000\,\mu\varepsilon$ (measured at $L = 6\,\mathrm{m}$)

The amplitude of the hydraulic cylinder's motion was initially selected so that a material strain of $\pm 1700\,\mu\varepsilon$ was measured at the TE of the blade at $L = 12\,\mathrm{m}$ using strain gauges. This load level was increased subsequently and after approximately 11000 cycles of the final FLL 3, the test was terminated due to the growth of a structurally critical crack at the LE, which most likely occurred due to fiber failure.

For the analysis of the different rotor blade states in between and after the application of the FLLs, dynamic tests were performed. These tests were carried out using dynamic shaker excitations, during which the rotor blade was decoupled from the hydraulic cylinder unit so that its motion was free of this constraint. The shaker was connected to load shear 2 at $L = 15\,\mathrm{m}$. Each excitation was carried out in the edgewise direction using broadband white noise and lasted approximately 20 minutes. Table 3 provides an overview of the rotor blade states together with a description of the corresponding rotor blade's condition with respect to structural integrity. Figures 3 and 4 show photographs of the described fatigue cracks that occurred during the course of the test.

https://doi.org/10.5194/wes-2025-219
Preprint. Discussion started: 6 November 2025

eawe european academy of wind energy
Open Access WIND ENERGY SCIENCE DISCUSSIONS

Table 3. Analysis states of the laboratory rotor blade to which shaker excitations were applied.

State	Date	Fatigue load level (FLL)	Description
I	04/22/2021	State after FLL 1	Vertical cracks across the TE.
II	04/26/2021	State after FLL 2	More vertical cracks across the TE.
III	04/29/2021	State after FLL 3	Crack across the LE at $L = 8\,\mathrm{m}$.

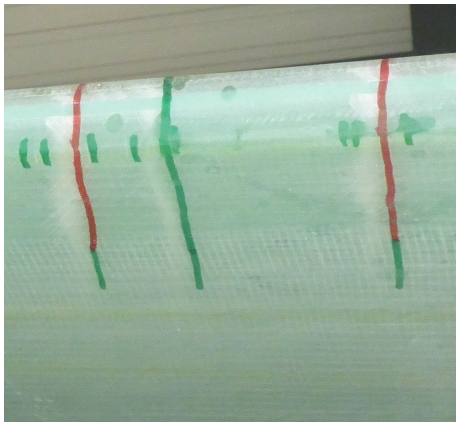

Figure 3. Vertical cracks across the TE traced out in red for state I and in green for state II.

(a) Zoomed out.

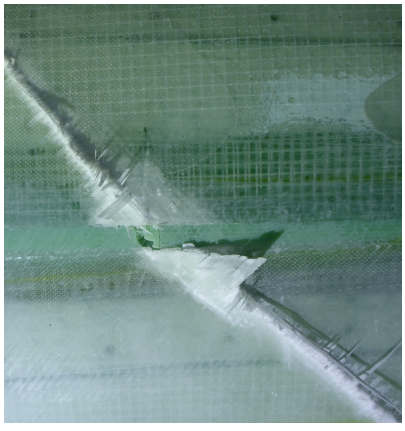

(b) Zoomed in.

Figure 4. Crack across the LE at $L = 8\,\mathrm{m}$ in state III.

3.1 Operational modal analysis

In this work, Bayesian operational modal analysis (BayOMA) (Au et al., 2013) is utilized for the identification of the modal parameters from the measurement data of the dynamic tests under broudband white noise excitation. The sampling rate was set to $100\,\mathrm{Hz}$ during the measurements. Figure 5 illustrates the frequency spectrum including the first $N_{\mathrm{modes}} = 5$ eigenfrequencies of an example acceleration time period of the large-scale rotor blade recorded in state I. The frequency ranges utilized for the BayOMA are highlighted.

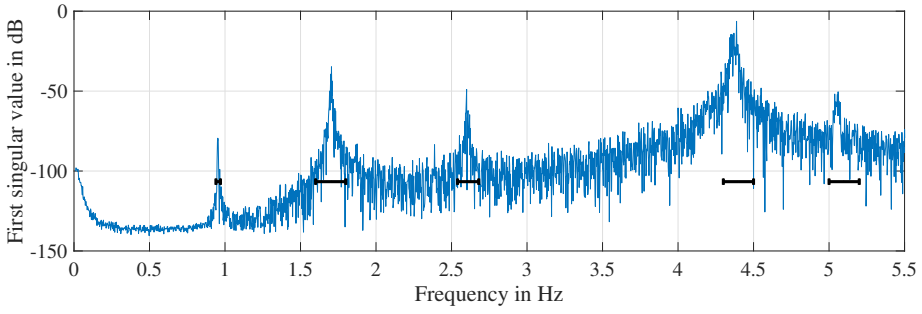

Figure 5. Frequency spectrum of the acceleration measurement in state I subject to broadband white-noise excitation. The frequency ranges utilized for the BayOMA are highlighted.

https://doi.org/10.5194/wes-2025-219
Preprint. Discussion started: 6 November 2025

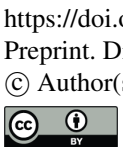

eawe european academy of wind energy
Open Access WIND ENERGY SCIENCE DISCUSSIONS

To visualize the stability and consistency of the recorded measurement data over time, the measurement data were segmented into a number of datasets N_{sets}. The evaluation time period was set to $T_{\text{Data}} = 400\,\text{s}$ and a moving window with an overlap of $385\,\text{s}$ was applied. For approximately $20\,\text{min} = 1200\,\text{s}$ total measurement time, this results in $N_{\text{sets}} = 53$ datasets. For each dataset, BayOMA was applied, resulting in 53 outputs which comprise the mean value and standard deviation of each eigenfrequency and the mean value and covariance matrix of each eigenmode. Figure 6 shows box plots of all eigenfrequency mean values $\overline{f}_{\text{M},i,j}$ identified from all 53 measurement datasets in the three different rotor blade states with $i \in [1, N_{\text{modes}}]$ and $j \in [1, N_{\text{sets}}]$.

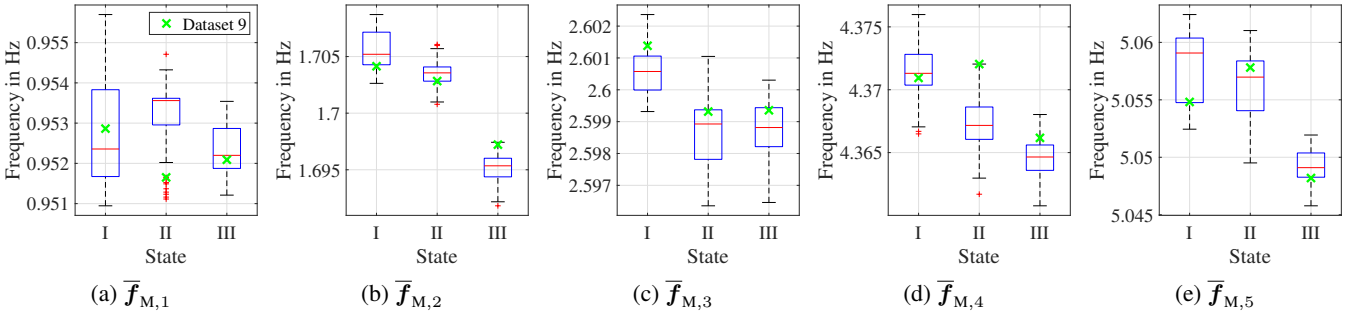

Figure 6. Box plots of the first five eigenfrequency mean values of the rotor blade identified for each measurement dataset in the three different analysis states using BayOMA. Box plot definitions: median (red line), interquartile range (blue box), extreme values (black whiskers) and outliers (red markers). Green crosses indicate the eigenfrequencies identified for dataset 9.

First of all, this analysis reveals that the interquartile ranges of the eigenfrequency mean values $\overline{f}_{\text{M},i}$ remain stable for each observed rotor blade state. This indicates consistent measurements with no significant fluctuations or outliers.

Looking more closely at the variation of the mean values of the five different eigenfrequencies across all states, it is clear that the eigenfrequencies $\overline{f}_{\text{M},1}$ and $\overline{f}_{\text{M},3}$, corresponding to flapwise bending mode shapes, are not significantly influenced by the damage that occurred during the fatigue test. In contrast, eigenfrequencies $\overline{f}_{\text{M},2}$, $\overline{f}_{\text{M},4}$ and $\overline{f}_{\text{M},5}$ exhibit a gradual reduction in magnitude, whereby the second and fourth eigenfrequencies correspond to edgewise bending mode shapes. The relative deviations of the first five eigenfrequencies between states I and III range from $0.02\,\%$ to $0.6\,\%$.

The measured acceleration time series together with the BayOMA results of the three rotor blade states are published as open-access resources alongside this work within the public data repository of Leibniz University Hanover (Wolniak et al., 2025b).

3.2 Finite element models

As both production and testing were carried out by Fraunhofer IWES, an outstanding feature of this rotor blade fatigue test was the complete documentation of the manufacturing process in addition to material and geometric data. Based on this detailed information, two different finite element (FE) models were developed and employed for the model-updating procedures presented in this work. The simulations were performed using the FE analysis software Abaqus. Both numerical models are illustrated in Figure 7. Further information regarding the element types, number of FEs and the computing time for the modal

https://doi.org/10.5194/wes-2025-219
Preprint. Discussion started: 6 November 2025

eawe european academy of wind energy
Open Access WIND ENERGY SCIENCE DISCUSSIONS

analysis is given in Table 4, whereby the computing time comprises the setup of the model itself (i.e., the input file) and the modal analysis.

Firstly, a beam model was created based on the available cross-sectional characteristics of the rotor blade. Two-node linear beam elements, available in Abaqus as B31 elements, are selected, whereby a total of 251 beam elements are utilized. The B31 elements are based on the Euler-Bernoulli beam theory, allowing the representation of bending, axial, and torsional deformations along the beam axis. The varying sectional properties were assigned to the beam elements using general cross-sectional parameters. The load shears were simplified as point masses according to the information listed in Table 1 and assigned to the structure using concentrated mass elements in Abaqus.

Secondly, a detailed shell model was set up based on the geometric data and composite layup available from the manufacturing process documentation. For this numerical model, S3R (three-node triangular) and S4R (four-node quadrilateral) shell elements with reduced integration were utilized. These elements efficiently capture bending, membrane, and transverse shear behavior, making them suitable for modeling thin to moderately thick shell structures. The load shears were modeled in detail using C3D4 tetrahedral solid elements and were included in all subsequent calculations, as they were attached during the whole experiment. In total, the shell model comprises approximately 310000 FEs, of which around 81700 are shell elements.

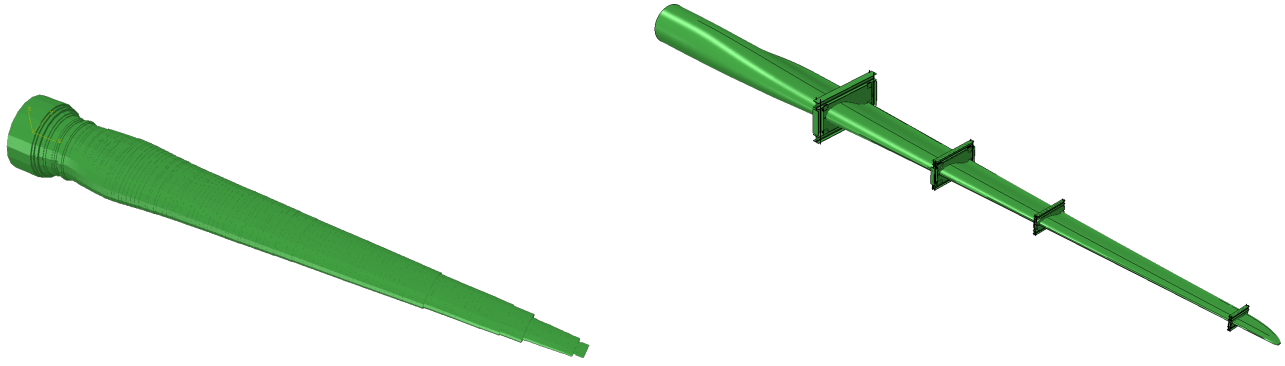

(a) Beam model. (b) Shell model.

Figure 7. FE models of the 31 m wind turbine rotor blade.

Table 4. Information regarding the two FE models utilized for the model updating of the laboratory rotor blade.

FE model	Element notation in Abaqus	Representation of the load shears	Number of FEs	Computing time for the modal analysis
Beam model	B31	Simplified using point masses (MASS)	251	0.3 min
Shell model	S3R, S4R	Detailed using solid elements (C3D4)	310000	8 min

https://doi.org/10.5194/wes-2025-219
Preprint. Discussion started: 6 November 2025

eawe european academy of wind energy
Open Access WIND ENERGY SCIENCE DISCUSSIONS

4 Results

The following subsections present the results of the SDMU approach, applied using the three different design variable configurations (cf. Sections 2.1.1, 2.1.2 and 2.1.3) with the objective of identifying damage in the considered laboratory rotor blade. For this purpose, all available rotor blade states listed in Table 3 are considered and systematically combined, yielding a total of six different state combinations. These combinations are summarized in Table 5, whereby the combinations along the diagonal represent self-comparisons of identical states.

In this work, the SDMU approach is applied to three different design variable configurations, which feature different numbers of design variables N_{DVs}, each defining a damage distribution function. These configurations are associated with the two numerical models of different levels of detail. The upper and lower bounds $\boldsymbol{x}_{\text{ub}}$ and $\boldsymbol{x}_{\text{lb}}$ and physical units used for each design variable configuration are listed in Table 6.

Table 5. Rotor blade state combinations considered for the damage identification using the SDMU approach.

	State I	State II	State III
State I	I-I	I-II	I-III
State II		II-II	II-III
State III			III-III

Table 6. Upper and lower bounds for the different design variable configurations.

FE model	N_{DVs}	Units	$\boldsymbol{x}$	$\boldsymbol{x}_{\text{lb}}$	$\boldsymbol{x}_{\text{ub}}$
Beam model	3	$\begin{pmatrix}\text{m}\\ \text{m}\\ \text{-}\end{pmatrix}$	$\begin{pmatrix}\mu_L\\ \sigma_L\\ D_{\text{1D}}\end{pmatrix}$	$\begin{pmatrix}0\\ 0.001\\ -0.02\end{pmatrix}$	$\begin{pmatrix}31\\ 2\\ 0.02\end{pmatrix}$
Beam model	4	$\begin{pmatrix}\text{m}\\ \text{m}\\ \text{-}\\ \text{-}\end{pmatrix}$	$\begin{pmatrix}\mu_L\\ \sigma_L\\ D_{\text{1D}}\\ \lambda\end{pmatrix}$	$\begin{pmatrix}0\\ 0.001\\ -0.02\\ 0\end{pmatrix}$	$\begin{pmatrix}31\\ 2\\ 0.02\\ 1\end{pmatrix}$
Shell model	5	$\begin{pmatrix}\text{m}\\ \text{m}\\ \text{-}\\ \text{-}\\ \text{-}\end{pmatrix}$	$\begin{pmatrix}\mu_L\\ \sigma_L\\ \mu_P\\ \sigma_P\\ D_{\text{2D}}\end{pmatrix}$	$\begin{pmatrix}0\\ 0.001\\ -0.5\\ 0.01\\ -0.02\end{pmatrix}$	$\begin{pmatrix}31\\ 2\\ 0.5\\ 0.3\\ 0.02\end{pmatrix}$

For all model-updating procedures conducted in this work, the two objectives involve the minimization of the discrepancies in both the first $N_{\text{modes}} = 5$ eigenfrequencies and eigenmodes between those identified from the measurement data and those calculated using the respective FE models. For the sample provision within the SDMU approach, the $N_{\text{sets}} = 53$ modal parameter mean values identified for each reference and analysis (i.e., target) state are cross-combined using the Cartesian product. This results in a total of $N_{\text{SP}} = N_{\text{sets}}^2 = 2809$ input samples and, consequently, in the same number of functions N_{sets}^2 representing the two objectives (cf. Equation 13). The subsequent numerical optimization is carried out using the deterministic multi-objective global pattern search (MOGPS) algorithm. Accordingly, the present work employs a fully deterministic SDMU realization for the damage identification on the laboratory rotor blade.

Importantly, the input samples directly represent the identified modal parameter mean values of each dataset. As demonstrated in Section 3.1, the measurement conditions were stationary, i.e., no significant variations in temperature, humidity or other environmental factors occurred during the rotor blade fatigue test. Consequently, the generated sample set inherently reflects the frequentist uncertainty associated with the measurement and modal identification process. For applications involving significant environmental or operational variations, however, this sampling strategy would no longer be sufficient and an

https://doi.org/10.5194/wes-2025-219
Preprint. Discussion started: 6 November 2025

eawe european academy of wind energy
Open Access WIND ENERGY SCIENCE DISCUSSIONS

alternative sample provision approach, for example based on the variance estimates provided by BayOMA, would be required to account for the additional sources of uncertainty.

For the visualization of the results, cumulative distribution functions (CDFs) are utilized. The CDFs are calculated based on the respective optimal design variables associated with the Pareto frontier, which is the result of the multi-objective optimization (i.e., model updating) procedure employed in this work. A CDF provides a comprehensive view of how probabilities are distributed across the range of the considered (design) variable. A notable feature of CDFs is the rate at which they increase. A steep section in a CDF indicates a rapid accumulation of probability over a small range of values. This indicates that a significant portion of the data points are concentrated around that region. Consequently, the probability density function (PDF), which is the derivative of the CDF, will be high in this area, pointing to a high density of occurrences.

4.1 Model-updating results using the beam model

To begin with, the damage identification results obtained using the beam model of the rotor blade (cf. Figure 7a) are presented for the three- and four-dimensional design variable configurations, as introduced in Sections 2.1.1 and 2.1.2, respectively. Before the application of the SDMU approach, preliminary studies are conducted to determine suitable settings for the input data and optimization algorithm hyperparameters. These studies are carried out using the three-dimensional design variable parameterization defined for the beam model with upper and lower bounds according to Table 6.

4.1.1 Settings

The first step of the SDMU approach is a single deterministic model-updating run using the numerical model, in this case, the beam model of the rotor blade. The resulting samples and corresponding modal parameters serve as the input data for the subsequent meta-model setup. Therefore, appropriate settings have to be defined for this initial deterministic model-updating run forming the basis of the subsequent (meta)SDMU procedure.

Regarding the utilized MOGPS optimization algorithm, two hyperparameters exist, namely the maximum number of objective function evaluations N_{evals} and the algorithm-specific number of tracked globally best coordinates T (Hofmeister et al., 2019). To evaluate which settings of N_{evals} and T are suitable, a convergence study is set up. To this end, a set of $N_{\text{test}} = 500$ design variable samples is randomly generated in the design variable space (cf. Table 6) and the corresponding modal parameters are calculated using the beam model. These results are utilized as test data to evaluate each meta-model, set up using different combinations of N_{evals} and T. The evaluation of each combination is calculated using the cumulated relative root mean square error (RMSE) of the first $N_{\text{modes}} = 5$ eigenfrequencies

$$\varepsilon_{\text{meta},f} = \sum_{i=1}^{N_{\text{modes}}} \left(\sqrt{\frac{1}{N_{\text{test}}} \sum_{j=1}^{N_{\text{test}}} \left(\frac{f_{\text{meta,S},i}(\boldsymbol{x}_{\text{1D},j}) - f_{\text{S},i}(\boldsymbol{x}_{\text{1D},j})}{f_{\text{S},i}(\boldsymbol{x}_{\text{1D},j})} \right)^2} \right). \tag{15}$$

https://doi.org/10.5194/wes-2025-219
Preprint. Discussion started: 6 November 2025

eawe european academy of wind energy
Open Access WIND ENERGY SCIENCE DISCUSSIONS

Figure 8 shows a heat map according to the natural logarithm of the eigenfrequency error $\varepsilon_{\text{meta},f}$. The minimum error is obtained for $T = 200$ and $N_{\text{evals}} = 5000$, which are therefore selected as the hyperparameter settings for the model-updating run used to populate the meta-model. Notably, the meta-model error remains consistently low for $T \geq 200$ and $N_{\text{evals}} \geq 2000$.

For the initial deterministic model-updating run, only a single set of modal parameters can be used as input in the objective functions (cf. Equation 13). As discussed in Section 3.1, the measurements show a high level of consistency without significant fluctuations or outliers. Consequently, the specific choice of the modal parameters used as input for the initial model-updating run is not critical. In this work, the modal parameters identified from the measurement data after a 2-minute settling time are selected, corresponding to dataset number 9. The corresponding eigenfrequency mean values are marked in Figure 6 with green crosses.

To verify that this set of modal parameters is indeed representative, model-updating runs with $T = 200$ and $N_{\text{evals}} = 5000$ are performed for all available datasets, shown as an example for combination I-III (cf. Table 5). In this context, a one-to-one mapping is employed. Figure 9 shows all $N_{\text{sets}} = 53$ resulting CDFs for the three design variables. The results demonstrate that the choice of the input dataset has no significant effect on the model-updating results, confirming that the chosen dataset 9 (highlighted in green) is representative. Consequently, $j = 9$ is used in Equation 13 for evaluating the two objective functions within the deterministic model-updating runs.

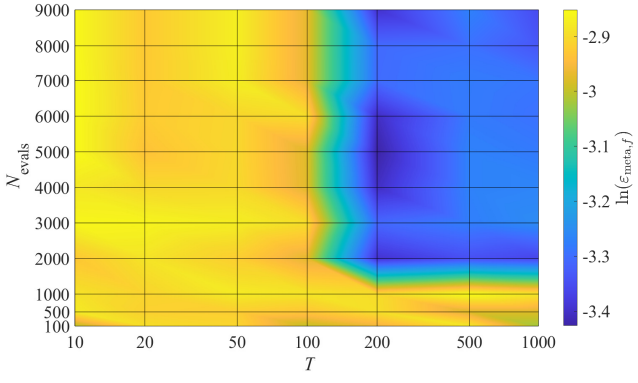

Figure 8. Evaluation of each meta-model set up using different combinations of N_{evals} and T. Surface colored according to the error $\ln(\varepsilon_{f,\text{meta}})$.

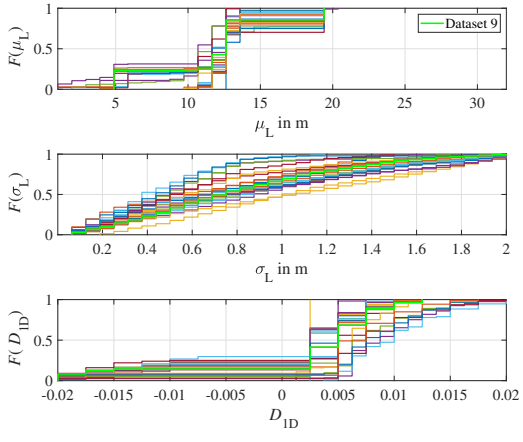

Figure 9. Resulting CDFs of the deterministic model-updating procedures for combination I-III based on the modal parameters of all datasets. The results for dataset 9 are highlighted in green.

Table 7. Settings for the SDMU procedure.

	Equation	Settings	FE model evaluations
Setup meta-model	13, $j = 9$	$N_{\text{evals}} = 5000$ $T = 200$	5000
MetaSDMU	13, $j \in [1, N_{\text{sets}}^2]$	$N_{\text{evals}} = 5000$ $T = 20$	

https://doi.org/10.5194/wes-2025-219
Preprint. Discussion started: 6 November 2025

eawe european academy of wind energy
Open Access WIND ENERGY SCIENCE DISCUSSIONS

4.1.2 Results for 3 design variables

This section presents the results obtained with the (meta)SDMU approach using the three-dimensional design variable configuration, which defines the one-dimensional damage distribution function applied to the beam model. For each state combination, the design variable samples and corresponding eigenfrequencies and eigenmodes from the initial deterministic model-updating runs serve as input for the meta-models, using the hyperparameter settings determined previously. Based on these meta-models and by applying Equation 14, the metaSDMU procedure is carried out. As noted earlier, the $N_{\text{sets}} = 53$ identified eigenfrequency and eigenmode mean values constitute the input samples and are cross-combined. This results in $N_{\text{sets}}^2 = 2809$ two-objective functions, forming the basis of 2809 model-updating runs per combination, all of which are based on the corresponding meta-models.

Figure 10 shows the resulting CDFs for each design variable of each combination. The CDFs are derived from all optimal design variables obtained in the course of all N_{sets}^2 model-updating runs. For the combinations I-III and II-III, where state III represents the target state with the emerged crack at the TE of the rotor blade, the correct crack location and extent are highlighted in addition to the results for the design variables μ_L and σ_L. The crack extends longitudinally from $\mu_L = 7.5\,\text{m} - 8.5\,\text{m}$, yielding a correct damage width of $1\,\text{m}$. As the one-dimensional damage distribution function is formulated based on a Gaussian distribution function (cf. Section 2.1.1), $\mu_L \pm 1\sigma_L$ represents the range including approximately $68\,\%$ of the data values, whereas $\mu_L \pm 2\sigma_L$ corresponds to roughly $95\,\%$ of the values. Consequently, $2\sigma_L$ is associated with the correct damage extent of $\pm 0.5\,\text{m} = 1\,\text{m}$, resulting in a correct value for $1\sigma_L = 0.25\,\text{m}$. Both values are highlighted in Figure 10b. For the self-combinations I-I, II-II and III-III, the known zero-damage intensity is highlighted in addition to the design variable D_{1D}. Moreover, the red crosses indicate a representative optimal design variable vector $\boldsymbol{x}_{\text{1D,optimal}}$ that is selected from the CDFs such that the first design variable, the damage position μ_L, is set to its median value $\tilde{\mu}_L$, defined as the $50\,\%$ value of the corresponding CDF.

https://doi.org/10.5194/wes-2025-219
Preprint. Discussion started: 6 November 2025

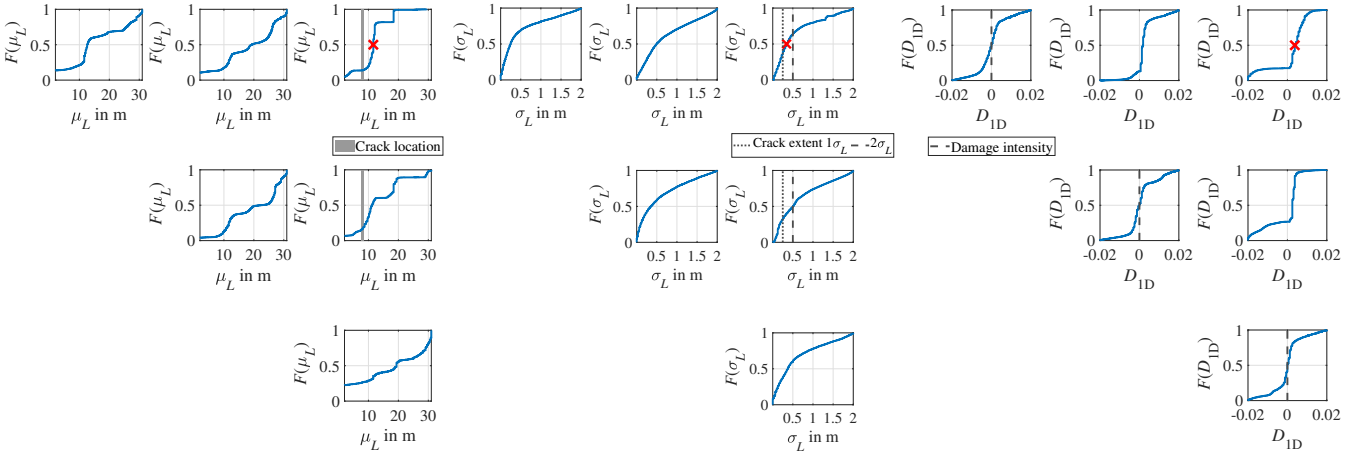

(a) Design variable μ_L. (b) Design variable σ_L. (c) Design variable D_{1D}.

Figure 10. Resulting CDFs of the SDMU approach applied to the beam model using the one-dimensional damage distribution function parameterized by three design variables, with settings given in Table 7. The red crosses added for combination I-III indicate an example optimal design variable vector.

Starting with combinations I-I, II-II and III-III, where each state is compared with itself, the model-updating results are expected to reflect the absence of damage. The corresponding CDFs of the damage intensity D_{1D}, shown in Figure 10c, are nearly identical, with $D_{1D} = 0$ being the most probable outcome for all three self-comparisons. The results for design variable μ_L, shown in Figure 10a, are also similar to each other, showing a sample distribution across the entire design variable space without clear probability clusters. Likewise, the longitudinal damage extent σ_L shown in Figure 10b exhibits a similar pattern with a slightly steeper slope for $\sigma_L < 0.5$. Although the damage position and extent are not directly relevant when the damage intensity is zero, the lack of convergence in μ_L further confirms that no damage is present when these states are compared with themselves. In summary, with $D_{1D} = 0$ as the most probable solution, the results for combinations I-I, II-II and III-III consistently and correctly indicate that no damage is present in the rotor blade for these self-comparisons.

For combination I-II, comparing reference state I with analysis state II, no distinct damage position is apparent, as the design variable μ_L remains distributed across the design variable space. A similar pattern is observed for σ_L, again with a slightly steeper increase of the CDF for $\sigma_L < 0.5$. However, the damage intensity D_{1D} shifts slightly from $D_{1D} = 0$ to $D_{1D} \approx 0.002$ (cf. Figure 10c). This indicates that damage has occurred but no distinct position can be determined. This outcome is consistent with the target rotor blade state II, where numerous small vertical cracks appeared along the TE (cf. Figure 3). Consequently, no single location is severely damaged, instead, the stiffness of the rotor blade is slightly reduced along the entire blade length due to these minor cracks.

Examining combinations I-III and II-III, where state III represents the target state with the most severe damage, the optimal damage intensity shifts to $D_{1D} \approx 0.005$. This positive value corresponds to a stiffness reduction in the rotor blade beam model according to the applied one-dimensional damage distribution function. The location of the stiffness reduction is identified at $\mu_L \approx 11 - 12\,\mathrm{m}$ for both combinations, which overestimates the actual damage location ($L = 7.5 - 8.5\,\mathrm{m}$) by approximately $3 - 4\,\mathrm{m}$. The results for the damage width σ_L, shown in Figure 10b, are again spread across the design variable space. Compared

https://doi.org/10.5194/wes-2025-219
Preprint. Discussion started: 6 November 2025

eawe european academy of wind energy
Open Access WIND ENERGY SCIENCE DISCUSSIONS

to the solutions for all other combinations, the CDFs for combinations I-III and II-III show a noticeably steeper slope for $\sigma_L < 0.5\,\mathrm{m}$, whereby the median value lies exactly between the $1\sigma_L$ and $2\sigma_L$ values highlighted in the figure. Consequently, this identified damage extent corresponds reasonably well with the actual crack length of approximately $1\,\mathrm{m}$.

To summarize, the SDMU procedure yields very similar results for combinations I-III and II-III, comparing states I and II to the same target state III. Moreover, for the self-combinations I-I, II-II and III-III, the model-updating procedure consistently returns zero-damage results. These findings demonstrate the consistency and, consequently, the reliability of the applied SDMU approach, objective function formulation and utilized design variable configuration.

To illustrate a representative damage distribution (i.e., stiffness reduction) for combination I-III, an example optimal design variable vector $\boldsymbol{x}_{\mathrm{1D,optimal}}$ is selected from the CDFs such that the first design variable is set to its median value $\tilde{\mu}_L$. The remaining two design variables are chosen as the optimal values corresponding to this fixed first design variable, which, in the case of the beam model, also coincide with their respective median values. In Figure 10, the example optimal design variable vector $\boldsymbol{x}_{\mathrm{1D,optimal}}$ is indicated using red crosses. The stiffness reduction resulting from the one-dimensional damage distribution function based on $\boldsymbol{x}_{\mathrm{1D,optimal}}$ is visualized in Figure 11. For comparison, Figure 12 visualizes the actual damage due to the crack that emerged at $L \approx 8\,\mathrm{m}$ (cf. Figure 4). It is evident that the crack location is overestimated by approximately $3.5\,\mathrm{m}$.

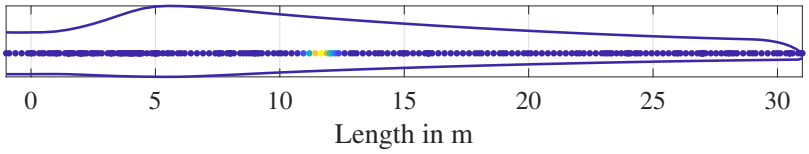

Figure 11. Visualization of the stiffness reduction based on $\boldsymbol{x}_{\mathrm{1D,optimal}}$, denoted by red crosses in Figure 10, in the beam model. The schematic rotor blade geometry is additionally outlined.

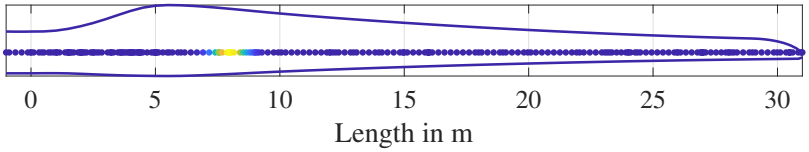

Figure 12. Visualization of the correct stiffness reduction in the beam model. The schematic rotor blade geometry is additionally outlined.

4.1.3 Results for 4 design variables

The results obtained using the four-dimensional parameterization of the one-dimensional damage distribution function, adding a separate consideration of the stiffness alterations in flapwise and edgewise directions via the design variable λ, are generally consistent with those presented above. Figure 13 shows the resulting CDFs of all optimal design variables for the six state combinations. As before, for combinations I-III and II-III, the correct damage location and extent are highlighted in addition to the results for the design variables μ_L and σ_L. Moreover, the zero-damage results for all three self-comparisons are highlighted in addition to the results for the design variable D_{1D}.

https://doi.org/10.5194/wes-2025-219
Preprint. Discussion started: 6 November 2025

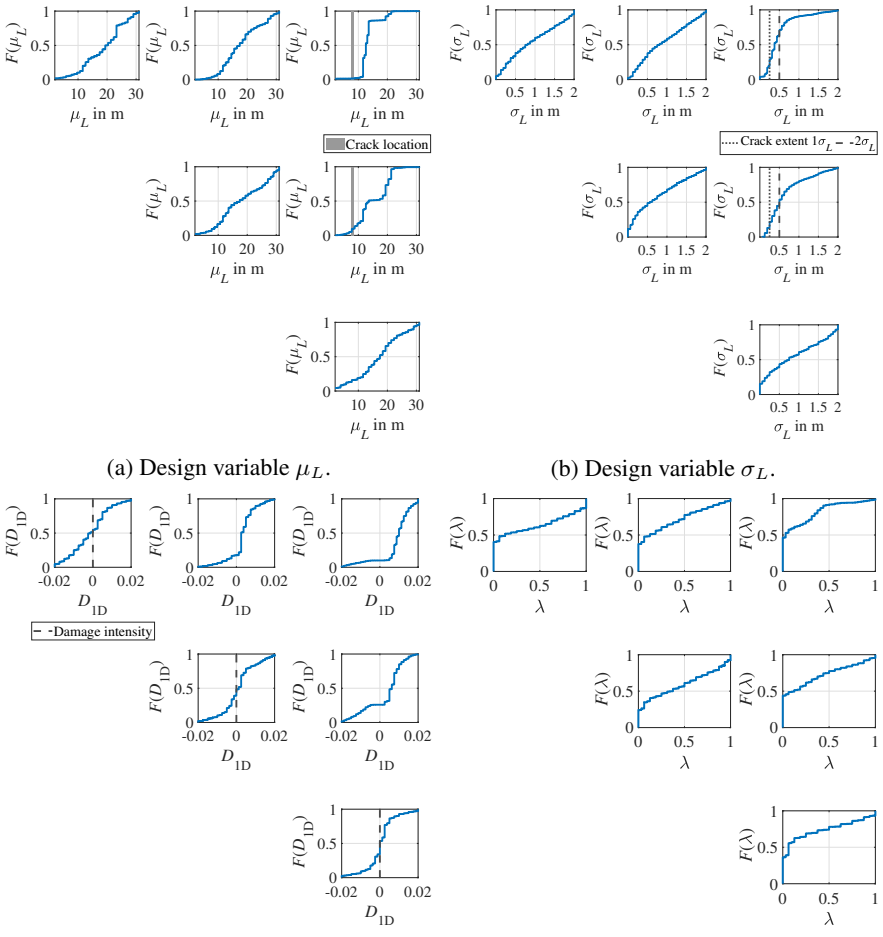

(a) Design variable μ_L.

(b) Design variable σ_L.

(c) Design variable D_{1D}.

(d) Design variable λ.

Figure 13. Resulting CDFs of the SDMU approach applied to the beam model using the one-dimensional damage distribution function parameterized by four design variables, with settings given in Table 7.

Again, the design variable D_{1D}, shown in Figure 13c, returns zero as the most probable outcome for all three self-comparisons and indicates a stiffness reduction for combinations I-II, I-III and II-III. Closer examination reveals that the stiffness reduction increases from combination I-II to I-III and remains similar between combinations I-III and II-III. This is consistent with the observations from Figure 10c. Similarly, the design variables μ_L and σ_L yield comparable results for the two design variable configurations applied to the beam model of the laboratory rotor blade.

Regarding the definition of the fourth design variable λ (cf. Section 2.1.2), a value of $\lambda = 0$ implies a stiffness alteration applied in the edgewise direction and a value of $\lambda = 1$ implies a stiffness alteration applied in the flapwise direction. It is evident from Figure 13d that $\lambda = 0$ is the most probable solution for all combinations, indicating that mainly the stiffness in the edgewise direction is reduced, given that D_{1D} is positive. For combinations I-II, I-III and II-III, this probability reaches approximately $50\,\%$, while the self-comparisons show slightly less conclusive results.

https://doi.org/10.5194/wes-2025-219
Preprint. Discussion started: 6 November 2025

eawe european academy of wind energy
Open Access WIND ENERGY SCIENCE DISCUSSIONS

Consequently, the separate consideration of the edgewise and flapwise directions captures the directional effect of the damage and provides an approximate indication of its positioning along the blade perimeter. However, the results should not be interpreted as ideal, since even in the self-comparison a significant probability of $\lambda = 0$ is observed. Therefore, these findings should not be overemphasized. A true assessment of directional dependence would require the use of a shell model, which is presented in the following subsection.

4.2 Model updating using the shell model

Here, the damage identification results of the (meta)SDMU approach applied to the shell model of the laboratory rotor blade are presented. In this case, the two-dimensional damage distribution function parameterized by five design variables is utilized with upper and lower bounds according to Table 6.

In the initial deterministic model-updating run for each combination, the same settings as listed in Table 7 are employed. Based on the samples and corresponding eigenfrequencies and eigenmodes, the respective meta-models are created using the same settings as before. For the subsequent metaSDMU approach, only the maximum number of objective function evaluations is doubled to $N_{\text{evals}} = 10000$ as more evaluations are needed for a sufficient convergence of the design variables in a higher-dimensional design variable space. The number of tracked globally best coordinates is, again, selected in the same way as before to be $T = 20$.

Figure 14 shows the resulting CDFs obtained for each design variable of each combination. As before, these CDFs are calculated based on all optimal design variables identified in the course of all N_{sets}^2 separate model-updating runs for each input sample. For combinations I-III and II-III, the correct edgewise and flapwise locations of the emerged crack in state III are marked in gray. In addition, the 1σ and 2σ damage extents are highlighted for both directions. For all three self-comparisons, the zero-damage result is highlighted. Furthermore, the red crosses indicate a possible optimal design variable vector $\boldsymbol{x}_{\text{2D,optimal}}$ for combination I-III. This example optimal design variable vector is selected from the CDFs as before such that the first design variable, the damage position μ_L, is set to its median value $\tilde{\mu}_L$, defined as the $50\,\%$ value of the corresponding CDF.

https://doi.org/10.5194/wes-2025-219
Preprint. Discussion started: 6 November 2025

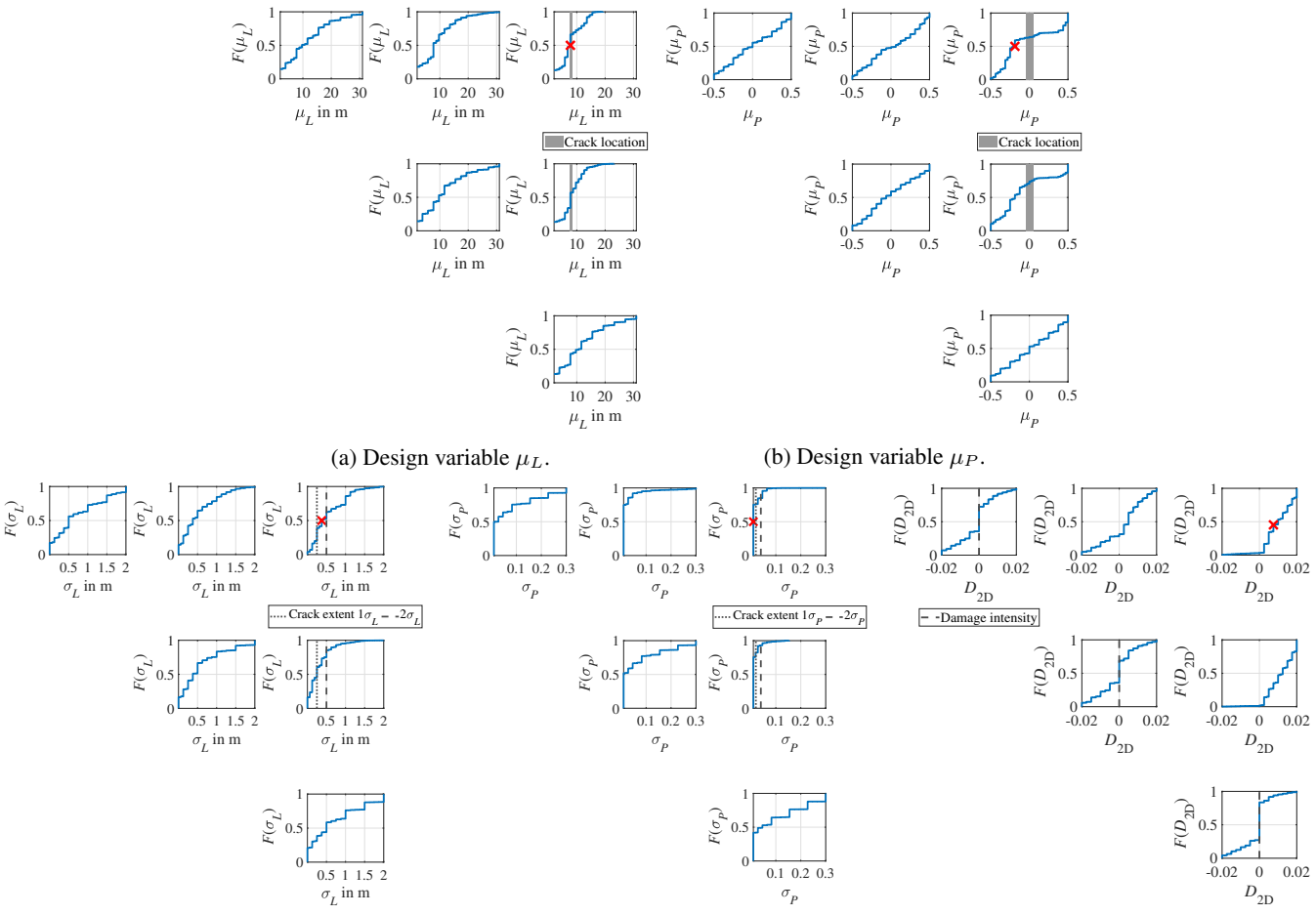

(a) Design variable μ_L. (b) Design variable μ_P.

(c) Design variable σ_L. (d) Design variable σ_P. (e) Design variable D_{2D}.

Figure 14. Resulting CDFs of the SDMU approach applied to the shell model using the two-dimensional damage distribution function parameterized by five design variables. The red crosses added for combination I-III indicate an example optimal design variable vector.

For the design variable μ_L, shown in Figure 14a, combinations I-III and II-III, with state III as the target state, clearly show that the damage localization along the blade length almost exactly matches the correct crack position. Most optimal values obtained using the shell model fall almost entirely in the shaded gray area, representing the true damage location. In contrast, the results obtained using the beam model (cf. Figures 10a and 13a) overestimate the damage position by approximately $3-4\,\mathrm{m}$. This means that the shell model improves localization accuracy along the blade length. For combination II-III, the CDF also shows a short steep section at $L = 8\,\mathrm{m}$. This indicates that the stiffness reduction has already begun at this location in state II, although it is less distinct than in state III. For combinations I-I, II-II and III-III, no clear convergence of μ_L is observed, which is consistent with the expected zero-damage result for these self-comparisons.

Figure 14b displays the resulting CDFs for the damage position μ_P along the blade perimeter. For combinations I-I, I-II, II-II and III-III, no clear convergence is visible, indicating that no specific position along the blade perimeter can be determined for these state combinations. For combinations I-III and II-III, a position between $\mu_P = -0.1$ and $\mu_P = -0.3$ is identified as

https://doi.org/10.5194/wes-2025-219
Preprint. Discussion started: 6 November 2025

eawe european academy of wind energy
Open Access WIND ENERGY SCIENCE DISCUSSIONS

the most probable solution. The negative sign corresponds to the pressure side of the blade, oriented upwards in the considered laboratory setup (cf. Figure 1). This outcome does not match the true crack location across the LE in state III, corresponding to $\mu_P = 0$ as marked in gray. However, closer inspection of Figure 4 shows that the crack propagates slightly more on the pressure side and changes direction through approximately $90°$ at this position. This may explain why the model-updating results identify the damage predominantly on the pressure side. Still, the damage localization along the blade perimeter remains complicated.

The results for the damage extent along the length σ_L, shown in Figure 14c, are similar to those obtained using the beam model (cf. Figures 10b and 13b) with the median lying exactly between the $1\sigma_L$ and $2\sigma_L$ values. The damage extent along the blade perimeter σ_P, shown in Figure 14d, indicates a rather small extent in this direction with the median being even lower than the highlighted $1\sigma_P$ value. Consequently, the optimal results for the covariance matrix $\mathbf{\Sigma}_{2D}$ correspond to a crack-like shape extenting in longitudinal direction. Whereas this reflects the characteristics of the real damage extent, the orientation does not correspond to the true extent across the LE of the rotor blade. However, it should be noted that an oblique damage extent, as is actually the case here (cf. Figure 4), cannot be captured by the currently applied covariance matrix $\mathbf{\Sigma}_{2D}$, since its off-diagonal terms are set to zero (cf. Section 2.1.3).

The results for the damage intensity D_{2D}, presented in Figure 14e, follow a pattern across all combinations similar to that observed for the (meta)SDMU results using the beam model (cf. Figures 10c and 13c). For the self-comparisons, $D_{2D} = 0$ is the most probable outcome. Combination I-II shows an initial stiffness reduction, which is visible due to the slight rightward shift of the CDF. For combination I-III, the CDF shifts further to the right, revealing a more distinct solution for a positive D_{2D}. This indicates an even greater stiffness reduction. The results for combination II-III, also targeting state III, show a comparable solution for D_{2D} ranging from 0.025 to 0.175.

The stiffness reduction corresponding to the optimal design variable vector $\boldsymbol{x}_{2D,optimal}$, marked in red in Figure 14, is visualized in Figure 15. Again, $\boldsymbol{x}_{2D,optimal}$ is selected with the first design variable set to its median value $\tilde{\mu}_L$, while the remaining four design variables are chosen as the optimal values corresponding to this fixed first design variable. For the shell model, these corresponding values coincide with the respective median values regarding design variables σ_L, μ_P and σ_P, whereas the corresponding optimal value for D_{2D} is slightly below its median. For comparison, Figure 16 shows the correct damage location associated with the crack that emerged in state III. It should be noted that the "correct" representation aligns with the intuitive perception of the crack extending across the LE. This does not correspond to the actual crack propagation, which runs obliquely across the LE (cf. Figure 4). However, as mentioned before, this obliqueness cannot be captured by the applied five-dimensional design variable parameterization, as the off-diagonal terms of the covariance matrix $\mathbf{\Sigma}_{2D}$ are set to zero (cf. Section 2.1.3).

In summary, the (meta)SDMU approach applied to the shell model of the rotor blade successfully localizes the damage along the blade length at $L \approx 8\,\mathrm{m}$. Furthermore, the damage exhibits an elongated, crack-like shape, which reflects the characteristics of the real damage extent. However, the found orientation is along the blade length rather than transverse to it and the circumferential damage position was not accurately captured at the LE of the rotor blade but shifted towards its pressure side.

https://doi.org/10.5194/wes-2025-219
Preprint. Discussion started: 6 November 2025

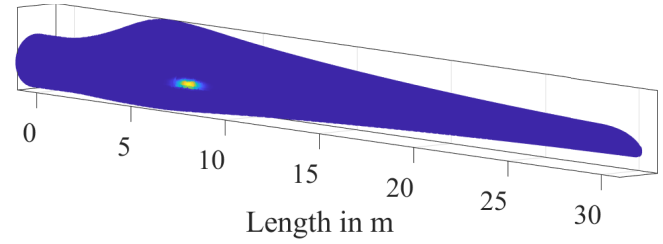

(a) View of the pressure side.

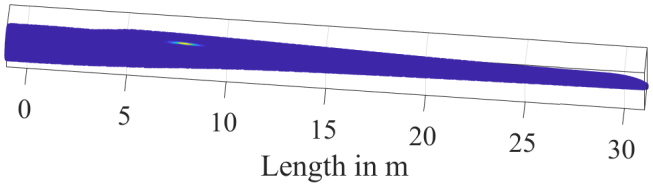

(b) View of the leading edge.

Figure 15. Visualization of the stiffness reduction based on $\boldsymbol{x}_{\text{2D,optimal}}$, denoted by red crosses in Figure 14, in the shell model.

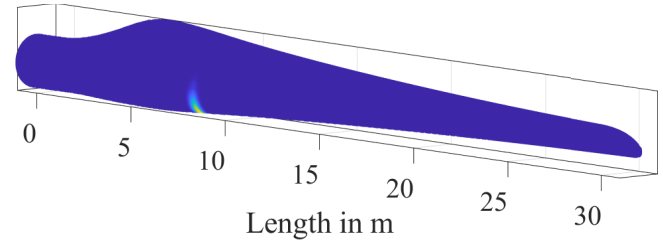

(a) View of the pressure side.

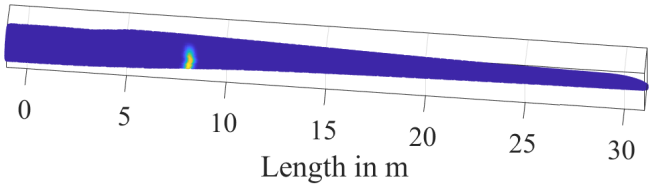

(b) View of the leading edge.

Figure 16. Visualization of the correct stiffness reduction in the shell model.

4.3 Comparison of the results

In this subsection, a direct comparison of the results obtained using the three different design variable configurations, defining the respective damage distribution functions applied to the two different numerical models, is presented. To illustrate this, Figure 17 shows all the CDFs resulting for combination I-III. This combination updates the reference state I to the analysis state III of the laboratory rotor blade.

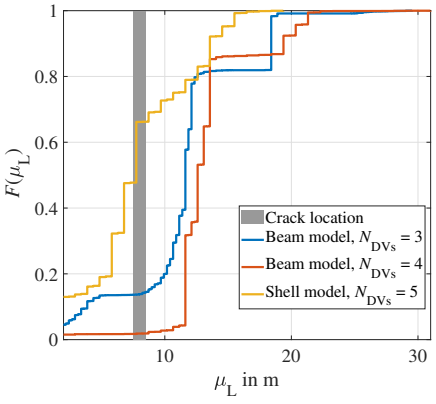

(a) Design variable μ_L.

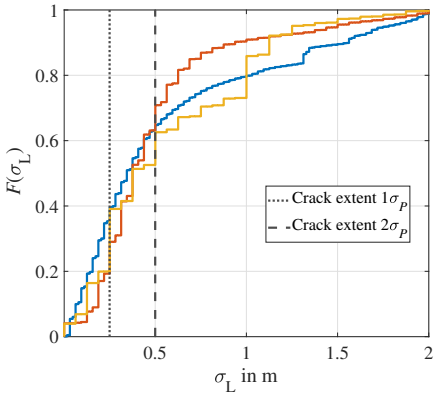

(b) Design variable σ_L.

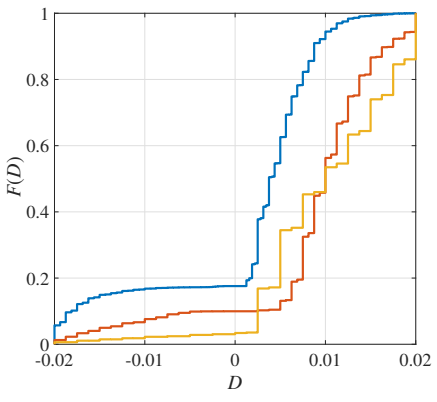

(c) Design variable D.

Figure 17. Resulting CDFs of the SDMU procedure for combination I-III – comparison of all three parameterizations of the damage distribution function.

https://doi.org/10.5194/wes-2025-219
Preprint. Discussion started: 6 November 2025

eawe european academy of wind energy
Open Access WIND ENERGY SCIENCE DISCUSSIONS

In general, the results for the three design variables μ_L, σ_L and D (i.e., D_{1D} and D_{2D}) show a high degree of similarity. This overall consistency confirms the methodological robustness of the presented (meta)SDMU approach and the validity of the three different implemented parameterizations of the damage distribution function. Moreover, the agreement across the results underlines their reliability, particularly given that two numerical models of distinctly different levels of accuracy and detail were employed.

However, upon closer inspection, some differences can be discerned. Most notably, the use of the more detailed shell model increases the accuracy of the damage localization along the blade length, shown in Figure 17a. Table 8 summarizes the localization accuracy of the different design variable parameterizations using the beam and shell models with respect to the true damage position $\hat{\mu}_L$ at $L = 8\,\mathrm{m}$ along the $31\,\mathrm{m}$ blade. Therefore, the medians $\tilde{\mu}_L$ – defined as the $50\,\%$ values of the CDFs – were calculated for each design variable configuration. To provide a quantitative metric for assessing the accuracy of the presented CDFs, Table 8 lists the relative error e_{μ_L} calculated in $\%$ per design variable configuration

$$e_{\mu_L} = 100 \times \frac{\hat{\mu}_L - \tilde{\mu}_L}{31\,\mathrm{m}}. \tag{16}$$

Table 8. Comparison of the damage localization accuracy.

FE model	N_{DVs}	$\tilde{\mu}_L$ in m	Deviation from $\hat{\mu}_L$ in m	e_{μ_L} in %
Beam model	3	11.63	3.63	11.7
Beam model	4	12.59	4.59	14.8
Shell model	5	7.75	0.25	0.8

The listed results demonstrate that the shell model reduces the damage localization error to less than $1\,\%$ of the blade length. Due to its higher spatial resolution and more detailed representation of the blade geometry, it is significantly more accurate in capturing local damage. However, this accuracy comes with the need for detailed geometric and material information and the cost of higher computational demand, with a computing time of around 8 minutes, including the input file generation, model loading and modal analysis. In contrast, the beam model provides a reasonably accurate damage localization within $11-15\%$ of the blade length despite its simplified representation, while requiring only around 20 seconds of computing time. This indicates that beam models can offer a practical compromise between computational efficiency and localization performance.

The damage extent is predicted nearly identically by all three parameterizations, illustrated in Figure 17b. The true longitudinal extent of the oblique crack propagation is approximately $1\,\mathrm{m}$, corresponding to a correct value of $2\sigma_L \approx 0.5\,\mathrm{m}$ and $1\sigma_L \approx 0.25\,\mathrm{m}$, as respectively indicated by the vertical dashed and dotted lines in the figure. All in all, the three model-updating procedures accurately reflect the predominantly local nature of the damage.

Regarding the results obtained for the damage intensity shown in Figure 17c, the beam model with 3 design variables predicts a slightly lower damage intensity, whereas the other two configurations yield similar results. Importantly, all three

https://doi.org/10.5194/wes-2025-219
Preprint. Discussion started: 6 November 2025

model-updating procedures consistently identify a stiffness reduction with high probability, indicating that the three presented damage parameterizations reliably capture the key structural effect of the damage.

5 Conclusions

In this work, FE model updating was performed with the objective of damage identification based on a laboratory rotor blade fatigue test. Three rotor blade states were measured during the test, resulting in six possible state combinations to which the presented model-updating procedure was applied. The sample-based deterministic model-updating (SDMU) approach was employed, which, in this particular application, accounts for identification uncertainty in the modal parameters. Three different design variable configurations were introduced, each defining a damage distribution function used to update the stiffness of two numerical models with different levels of fidelity (beam and shell). This methodological framework enabled a systematic evaluation of how model detail and design variable parameterization influence the results of model updating.

In summary, all three design variable configurations yielded consistent results across all six state combinations, confirming the robustness of the SDMU approach and validating the implemented parameterizations of the damage distribution function. The agreement among the results underlines their reliability, particularly given that two numerical models of distinctly different levels of accuracy and detail were employed. As expected, all model-updating procedures returned zero-damage results for the three self-comparisons and revealed a progressively increasing stiffness reduction together with a conclusive damage localization along the blade length. The most notable difference between the two utilized FE models was revealed with respect to the longitudinal damage localization. While the use of the shell model allows for a damage localization within less than $1\,\%$ of the blade length, the use of the beam model achieved an accuracy of only $11\,\%$, overestimating the true damage position by $3.5\,\mathrm{m}$.

The findings of this work underline the importance of defining the analysis objective in advance. Depending on whether precise localization or overall damage characterization is the primary goal, the choice of the numerical model and the associated design variable parameterization is decisive for obtaining meaningful and reliable results. In practice, this enables an informed balance between computational efficiency and model accuracy according to the desired outcome.

As the considered five-dimensional design variable parameterization applied to the shell model does not account for oblique damage extents, incorporating the off-diagonal terms of the covariance matrix represents an interesting extension. Future work should also aim to include model uncertainty in the SDMU approach. Moreover, the present study is limited to a laboratory experiment without realistic variation of environmental or operational conditions, which are of high relevance for rotor blades. Addressing these aspects will provide valuable extensions and enhancements to the presented model-updating approach.

Data availability. The measured acceleration time series together with the BayOMA results of the three rotor blade states are published as open-access resources alongside this work within the public data repository of Leibniz University Hanover: Wolniak et al. (2025b).

https://doi.org/10.5194/wes-2025-219
Preprint. Discussion started: 6 November 2025

eawe european academy of wind energy
Open Access WIND ENERGY SCIENCE DISCUSSIONS

Author contributions. Marlene Wolniak did the main research work. She prepared, installed, carried out, and analyzed the rotor blade test, set up the FE models, implemented and performed the model-updating procedure, evaluated the results and wrote the manuscript. Jasper Ragnitz contributed to the implementation of the model-updating framework, the interpretation of the data, and the evaluation. Clemens Jonscher assisted with the preparation and installation of the measurement campaign, performed the BayOMA, and contributed to the interpretation of the modal parameters. Benedikt Hofmeister supported the preparation and installation of the measurement campaign and acted as an assisting and consulting hand throughout all steps. Helge Jauken collaborated in conducting the rotor blade test, including preparation, installation, and execution, and was the main contributor to the development of the detailed shell model of the rotor blade. Through discussion and feedback, Clemens Hübler and Raimund Rolfes contributed to the interpretation and discussion of the results. All authors contributed to the revision of the manuscript and approved the final submitted version.

Competing interests. Raimund Rolfes is a member of the editorial board of the wind energy science journal.

Acknowledgements. We gratefully acknowledge the financial support of the Federal Ministry for Economic Affairs and Energy [research projects *MultiMonitorRB – Multivariate damage monitoring of rotor blades*, FKZ 0324157A, *MMRB-Repair-care – Multivariate damage monitoring of rotor blades: implementation and analysis of the effects of repair measures*, FKZ 03EE2043C, and *EMMA-Wind – Effiziente Messung und Monitoring von Windenergie-Anlagen*, FKZ 03EE3136B] and the financial support of the German Research Foundation (Deutsche Forschungsgemeinschaft, DFG) [SFB-1463-434502799], which have made this work possible. In addition, we gratefully acknowledge and would like to thank the Fraunhofer IWES that carried out the rotor blade manufacturing and provided the facilities for the full-scale testing of the wind turbine rotor blade in Bremerhaven.

https://doi.org/10.5194/wes-2025-219
Preprint. Discussion started: 6 November 2025

eawe european academy of wind energy
Open Access WIND ENERGY SCIENCE DISCUSSIONS

References

Algolfat, A., Wang, W., and Albarbar, A.: Damage Identification of Wind Turbine Blades - A Brief Review, Journal of Dynamics, Monitoring and Diagnostics, 2, https://doi.org/10.37965/jdmd.2023.422, 2023.

Au, S.-K., Zhang, F.-L., and Ni, Y.-C.: Bayesian operational modal analysis: Theory, computation, practice, Computers & Structures, 126, 3–14, https://doi.org/10.1016/j.compstruc.2012.12.015, 2013.

Avci, O., Abdeljaber, O., Kiranyaz, S., Hussein, M., Gabbouj, M., and Inman, D. J.: A review of vibration-based damage detection in civil structures: From traditional methods to Machine Learning and Deep Learning applications, Mechanical Systems and Signal Processing, 147, 107 077, https://doi.org/10.1016/j.ymssp.2020.107077, 2021.

Berger, R., Bruns, M., Ehrmann, A., Haldar, A., Häfele, J., Hofmeister, B., Hübler, C., and Rolfes, R.: EngiO – Object-oriented framework for engineering optimization, Advances in Engineering Software, 153, 102 959, https://doi.org/10.1016/j.advengsoft.2020.102959, 2021.

Bi, S., Beer, M., Zhang, J., Yang, L., and He, K.: Optimization or Bayesian Strategy? Performance of the Bhattacharyya Distance in Different Algorithms of Stochastic Model Updating, ASCE-ASME Journal of Risk and Uncertainty in Engineering Systems, Part B: Mechanical Engineering, 7, https://doi.org/10.1115/1.4050168, 2021.

Brownjohn, J.: Structural health monitoring of civil infrastructure, Philosophical Transactions of the Royal Society A: Mathematical, Physical and Engineering Sciences, 365, 589–622, https://doi.org/10.1098/rsta.2006.1925, 2007.

Bruns, M., Hofmeister, B., Grießmann, T., and Rolfes, R.: Comparative Study of Parameterizations for Damage Localization with Finite Element Model Updating, in: Proceedings of the 29th European Safety and Reliability Conference, pp. 1125–1132, https://doi.org/10.3850/978-981-11-2724-3_0713-cd, 2019a.

Bruns, M., Hofmeister, B., Hübler, C., and Rolfes, R.: Damage Localization Via Model Updating Using a Damage Distribution Function, in: Structural Health Monitoring 2019, pp. 909–917, https://doi.org/10.12783/shm2019/32202, 2019b.

Chetan, M., Yao, S., and Griffith, D. T.: Multi–fidelity digital twin structural model for a sub–scale downwind wind turbine rotor blade, Wind Energy, 24, 1368–1387, https://doi.org/10.1002/we.2636, 2021.

Das, S., Saha, P., and Patro, S. K.: Vibration-based damage detection techniques used for health monitoring of structures: a review, Journal of Civil Structural Health Monitoring, 6, 477–507, https://doi.org/10.1007/s13349-016-0168-5, 2016.

de Almeida, I. T., Lapa, G. V. P., Gay Neto, A., and de Almeida, S. F. M.: Design and extreme structural analysis of wind turbine blades: Beam and shell model comparison and discussion for a 10-MW reference turbine, Engineering Structures, 334, 120 155, https://doi.org/10.1016/j.engstruct.2025.120155, 2025.

Ereiz, S., Duvnjak, I., and Jiménez-Alonso, J. F.: Review of finite element model updating methods for structural applications, Structures, 41, 684–723, https://doi.org/10.1016/j.istruc.2022.05.041, 2022.

Faes, M. and Moens, D.: Recent Trends in the Modeling and Quantification of Non-probabilistic Uncertainty, Archives of Computational Methods in Engineering, 27, 633–671, https://doi.org/10.1007/s11831-019-09327-x, 2020.

Fan, W. and Qiao, P.: Vibration-based Damage Identification Methods: A Review and Comparative Study, Structural Health Monitoring, 10, 83–111, https://doi.org/10.1177/1475921710365419, 2011.

Friswell, M. I.: Damage identification using inverse methods, Philosophical Transactions of the Royal Society A: Mathematical, Physical and Engineering Sciences, 365, 393–410, https://doi.org/10.1098/rsta.2006.1930, 2007.

Friswell, M. I. and Mottershead, J. E.: Finite Element Model Updating in Structural Dynamics, vol. 38 of *Solid Mechanics and its Applications*, Springer Netherlands, ISBN 978-90-481-4535-5 978-94-015-8508-8, https://doi.org/10.1007/978-94-015-8508-8, 1995.

https://doi.org/10.5194/wes-2025-219
Preprint. Discussion started: 6 November 2025

Günther, C., Hofmeister, B., Hübler, C., Jonscher, C., Ragnitz, J., Schubert, J., and Steinbach, M. C.: Damage location in mechanical structures by multi-objective pattern search, Optim. Eng., https://doi.org/10.1007/s11081-024-09940-1, 2025.

Hau, E.: Wind Turbines, Springer Berlin Heidelberg, Berlin, Heidelberg, ISBN 978-3-642-27150-2, https://doi.org/10.1007/978-3-642-27151-9, 2013.

Hofmeister, B., Bruns, M., and Rolfes, R.: Finite element model updating using deterministic optimisation: A global pattern search approach, Engineering Structures, 195, 373 – 381, https://doi.org/10.1016/j.engstruct.2019.05.047, 2019.

Kaewniam, P., Cao, M., Alkayem, N. F., Li, D., and Manoach, E.: Recent advances in damage detection of wind turbine blades: A state-of-the-art review, Renewable and Sustainable Energy Reviews, 167, 112 723, https://doi.org/10.1016/j.rser.2022.112723, 2022.

Knebusch, J., Gundlach, J., and Govers, Y.: A SYSTEMATIC INVESTIGATION OF COMMON GRADIENT BASED MODEL UPDATING APPROACHES APPLIED TO HIGH-FIDELITY TEST-DATA OF A WIND TURBINE ROTOR BLADE, in: XI International Conference on Structural Dynamics, Proceedings of the XI International Conference on Structural Dynamics, pp. 2159–2174, EASDAthens, https://doi.org/10.47964/1120.9175.19508, 2020.

Kong, K., Dyer, K., Payne, C., Hamerton, I., and Weaver, P. M.: Progress and Trends in Damage Detection Methods, Maintenance, and Data-driven Monitoring of Wind Turbine Blades – A Review, Renewable Energy Focus, 44, 390–412, https://doi.org/10.1016/j.ref.2022.08.005, 2023.

Lake, R. C. and Nixon, M. W.: A preliminary investigation of finite-element modeling for composite rotor blades, in: Technical Memorandum, 1988.

Levin, R. I. and Lieven, N. A. J.: Dynamic Finite Element Model Updating Using Neural Networks, Journal of Sound and Vibration, 2010, https://doi.org/https://doi.org/10.1006/jsvi.1997.1364, 1998.

Link, M.: Updating of analytical models — review of numerical procedures and application aspects, in: Proc., Structural Dynamics Forum SD2000, pp. 193–223, Research Studies Press, Baldock, UK, 1999.

Marler, R. T. and Arora, J. S.: Survey of multi-objective optimization methods for engineering, Structural and Multidisciplinary Optimization, 26, 369–395, https://doi.org/10.1007/s00158-003-0368-6, 2004.

Mottershead, J. E. and Friswell, M. I.: Model updating in structural dynamics: a survey, Journal of Sound and Vibration, 167, 347–375, https://doi.org/10.1006/jsvi.1993.1340, 1993.

Mottershead, J. E., Link, M., and Friswell, M. I.: The sensitivity method in finite element model updating: A tutorial, Mechanical Systems and Signal Processing, 25, 2275–2296, https://doi.org/10.1016/j.ymssp.2010.10.012, 2011.

Noever-Castelos, P., Melcher, D., and Balzani, C.: Model updating of a wind turbine blade finite element Timoshenko beam model with invertible neural networks, Wind Energy Science, 7, 623–645, https://doi.org/10.5194/wes-7-623-2022, 2022.

Peeters, M., Santo, G., Degroote, J., and van Paepegem, W.: Comparison of Shell and Solid Finite Element Models for the Static Certification Tests of a 43 m Wind Turbine Blade, Energies, 11, 1346, https://doi.org/10.3390/en11061346, 2018.

Ragnitz, J., Hofmeister, B., Jonscher, C., Hübler, C., and Rolfes, R.: A stochastic multi-objective optimisation approach for damage localisation via model updating with uncertain input parameters, Engineering Structures, 330, 119 860, https://doi.org/10.1016/j.engstruct.2025.119860, 2025.

Simoen, E., De Roeck, G., and Lombaert, G.: Dealing with uncertainty in model updating for damage assessment: A review, Mechanical Systems and Signal Processing, 56-57, 123–149, https://doi.org/10.1016/j.ymssp.2014.11.001, 2015.

Timoshenko, S. P. and Gere, J. M.: Theory of elastic stability, Courier Corporation, 2012.

https://doi.org/10.5194/wes-2025-219
Preprint. Discussion started: 6 November 2025

Turnbull, H. and Omenzetter, P.: Fuzzy finite element model updating for damage severity assessment, Journal of Physics: Conference Series, 2647, 182 046, https://doi.org/10.1088/1742-6596/2647/18/182046, 2024.

Volovoi, V. V., Hodges, D. H., Cesnik, C. E. S., and Popescu, B.: Assessment of Beam Modeling Methods for Rotor Blade Applications, Mathematical and Computer Modeling, 33, 1099–1112, 2001.

Wernitz, S., Hofmeister, B., Jonscher, C., Grießmann, T., and Rolfes, R.: A new open–database benchmark structure for vibration–based Structural Health Monitoring, Structural Control and Health Monitoring, 29, https://doi.org/10.1002/stc.3077, 2022.

Wolniak, M., Hofmeister, B., Jonscher, C., Fankhänel, M., Loose, A., Hübler, C., and Rolfes, R.: Validation of an FE model updating procedure for damage assessment using a modular laboratory experiment with a reversible damage mechanism, Journal of Civil Structural Health Monitoring, 13, 1185–1206, https://doi.org/10.1007/s13349-023-00701-9, 2023.

Wolniak, M., Hofmeister, B., Dierksen, N., Ragnitz, J., Jonscher, C., Hübler, C., and Rolfes, R.: Uncertainty propagation via sample-based deterministic model updating for structural damage identification, https://doi.org/10.15488/19721, 2025a.

Wolniak, M., Jauken, H., Jonscher, C., Hofmeister, B., Ragnitz, J., and Rolfes, R.: Measurement data and BayOMA identification results of a 31 m wind turbine rotor blade, https://doi.org/10.25835/UWRCESYR, 2025b.

Worden, K., Farrar, C. R., Manson, G., and Park, G.: The fundamental axioms of structural health monitoring, Proceedings of the Royal Society A: Mathematical, Physical and Engineering Sciences, 463, 1639–1664, https://doi.org/10.1098/rspa.2007.1834, 2007.

Yang, W., Peng, Z., Wei, K., and Tian, W.: Structural health monitoring of composite wind turbine blades: challenges, issues and potential solutions, IET Renewable Power Generation, 11, 411–416, https://doi.org/10.1049/iet-rpg.2016.0087, 2017.